

Structure-Activity Relationships and Therapeutic Potential of Purinergic P2X7 Receptor Antagonists

Imane Ghafir El Idrissi,^a Sabina Podlewska,^b Carmen Abate,^{a,c} Andrzej J. Bojarski,^b Enza Lacivita,^{*a} Marcello Leopoldo^a

^aDipartimento di Farmacia - Scienze del Farmaco, Università degli Studi di Bari Aldo Moro, via Orabona, 4, 70125 Bari, Italy

^bMaj Institute of Pharmacology, Polish Academy of Sciences, 31-343 Kraków, 12 Smętna Street, Poland

^cConsiglio Nazionale delle Ricerche (CNR), Istituto di Cristallografia, via Amendola, 70125 Bari, Italy

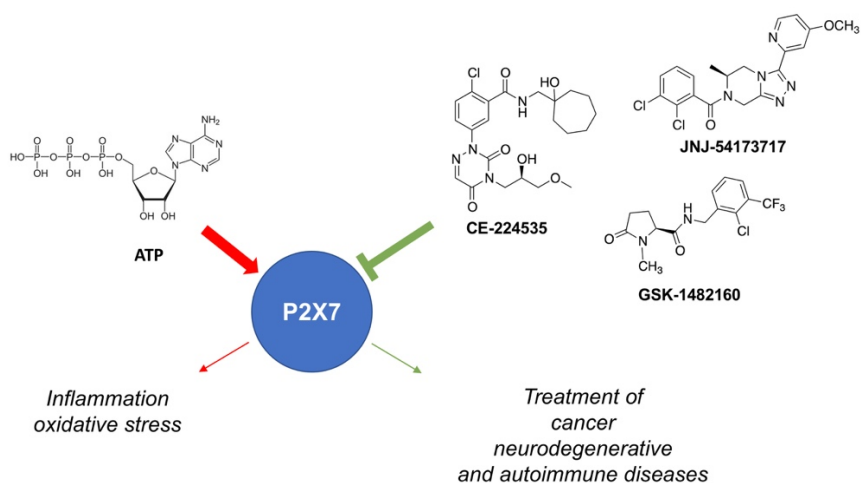
* Corresponding Author: Enza Lacivita, Dipartimento di Farmacia – Scienze del Farmaco, Università degli Studi di Bari Aldo Moro, via Orabona 4, 70125, Bari, Italy. E-mail: enza.lacivita@uniba.it; Phone: +39 080 5442750; Fax: +39 080 5442231

Abstract

The purinergic P2X7 receptor (P2X7R), an ATP-gated non-selective cation channel, is emerging as a gatekeeper of inflammation that controls the release of pro-inflammatory cytokines. As a key player in initiating the inflammatory signaling cascade, the P2X7 receptor is currently under intense scrutiny as a target for the treatment of different pathologies, including chronic inflammatory disorders (rheumatoid arthritis and osteoarthritis), chronic neuropathic pain, mood disorders (depression and anxiety), neurodegenerative diseases, ischemia, cancer (leukemia), and many others. For these reasons, pharmaceutical companies have invested in discovering compounds able to modulate the P2X7R and filed many patent applications.

This review article presents an account of P2X7R structure, function, and tissue distribution, emphasizing its role in inflammation. Next, we illustrate the different chemical classes of non-competitive P2X7R antagonists reported by highlighting their properties and qualities as clinical candidates for treating inflammatory disorders and neurodegenerative diseases. We also discuss the efforts to develop effective Positron Emission Tomography (PET) radioligands to progress the understanding of the pathomechanisms of neurodegenerative disorders, to provide evidence of drug-target engagement, and to assist clinical dose selection for novel drug therapies.

Graphical Abstract



Keywords: purinergic P2X7 receptor, inflammation, antagonists, neurodegenerative disorders, cancer, autoimmune diseases, Positron Emission Tomography

1. Introduction

The purinergic P2X7 receptor (P2X7R) belongs to the purinergic receptor family that includes the purine and pyrimidine receptors: the P1 adenosine receptors (A1, A2a, A2b, and A3), and the P2 family, which is further divided into the P2X (ionotropic) and P2Y (metabotropic) receptors. The ionotropic P2X receptor subfamily comprises seven subtypes of ATP-gated ion channels, termed P2X1-7 receptors [1, 2]. P2X7R is a non-selective cation channel activated by extracellular adenosine triphosphate (ATP) and it is expressed in the immune, peripheral, and central nervous systems and is implicated in ATP-mediated cell death and inflammation.

Over the last decade, tremendous efforts have been made by research groups from both industry and academia to develop structurally distinct P2X7R-specific antagonists as therapeutic agents [3, 4]. Much of the early efforts focused on treating diseases related to peripheral inflammation. Subsequently, there has been a shift toward developing brain penetrant antagonists for treating the chronic inflammatory status associated with neurological disorders [5], resulting in the identification of several clinical candidates, of which none has reached the market.

2. P2X7R molecular structure and activation mechanisms

The P2X7R is encoded by the *P2RX7* gene and it was first cloned and characterized in 1996 [6-8]. The gene encoding the P2X7R has been reported in at least 55 species. The P2X7R has been characterized in humans and six mammalian species, including macaque, dog, panda, mouse, rat, and guinea pig. The P2X7R of these species share 77-85% sequence identity with human P2X7R, while the sequence identity of the human P2X7R with non-mammalian species, such as the zebrafish, is below 40% [9]. The human P2X7R is highly polymorphic, and more than 150 single-nucleotide polymorphisms have been identified in the extracellular loop and the C-terminal domain [10-13], leading to diverse unpredictable functional consequences.

P2X7R is widely distributed in the mammalian body. Initially, it was thought that P2X7R distribution was restricted to hematopoietic lineage cells, such as macrophages, monocytes,

lymphocytes, and dendritic cells. Later, it became evident that P2X7R is also expressed by cells from other lineages, including fibroblasts, osteoblasts, endothelial cells, and epithelial cells. Moreover, P2X7R is expressed in the central and peripheral nervous system cells, such as microglia, astrocytes, oligodendrocytes, and Schwann cells [14]. P2X7R has also been reported in some populations of neurons, including those from the spinal cord, cerebellum, hypothalamus, and substantia nigra [15, 16].

Like other P2XRs, P2X7R forms trimeric assemblies of three identical subunits [17, 18]. Each subunit of the human P2X7R is a 595 amino acid-long protein [19] with a general architecture presenting a hydrophilic extracellular domain, two transmembrane helices (TM1 and TM2), and an intracellular part composed of the C-terminal and N-terminal regions [20, 21]. P2X7R has a carboxy-terminus much larger than other P2X family members with possible implications in regulating receptor function, including signaling pathways activation, cellular localization, protein-protein interactions, and post-translational modification [22].

The tridimensional structure of the P2X7R subunits resembles the shape of a dolphin, in which the extracellular part constitutes the dolphin body (with head and fins), whereas TM1 and TM2 constitute the dolphin tail. The structure consists of 8 alpha helices and 14 beta strands and it is stabilized by five conserved disulfide bonds (Fig. 1).

The assembly of the trimer forms the three ATP-binding pockets made of residues belonging to two complementary subunits (Fig. 2). The orthosteric binding pocket of P2X7R contains a high fraction of positively charged arginine and lysine, which is characteristic of the ATP binding sites on proteins. Between the two neighboring monomers, allosteric binding sites have been characterized so far [23-25] that can bind different compounds with inhibitory allosteric properties on the P2X7R activity (Fig. 2) [26]. Unlike the orthosteric binding site, the allosteric pockets are mainly formed by hydrophobic amino acids. A detailed description of the allosteric binding pocket is reported below. P2X7R is activated by very high ATP concentrations ($EC_{50} > 100 \mu\text{M}$) [27, 28], differently from the other P2XRs that show $EC_{50} \sim 10 \mu\text{M}$ [29]. Under physiological conditions, when ATP

concentration is low, P2X7R exists in the closed state. After a tissue insult or damage, the ATP concentration reaches high values ($> 100 \mu\text{M}$) in the milieu [30, 31], and three molecules of ATP bind to P2X7R, leading to receptor activation and consequent passage of Ca^{2+} , Na^+ , and K^+ across the plasma membrane causing an inward current and membrane depolarization [27, 32, 33].

Prolonged ATP stimulation does not cause receptor desensitization, as in other receptors, but induces cell death by opening membrane pores. The subsequent increase of membrane permeability allows the entrance into the cell of large hydrophilic molecules (900 Da) to hydrophilic solutes that impair homeostasis [34]. ATP hydrolysis and consequent decrease in concentration promote the closure of the pores [35].

3. P2X7R role in inflammation and related diseases

Activation of P2X7R by ATP leads to the activation of cell-type specific signaling pathways that include calcium mobilization, actin polymerization, chemotaxis, mediators release, cell maturation, cytotoxicity, and cell death [36]. One of the most studied signaling pathways associated with the P2X7R activation is the processing and externalization of the pro-inflammatory cytokine interleukin-1 β (IL-1 β) and its related family member interleukin-18 (IL-18). The cationic efflux through P2X7R, particularly the drop of intracellular K^+ concentrations, induces inflammasome complex assembly and subsequent pro-caspase-1 maturation into caspase-1 through the NOD-like receptor protein (NLRP3) [34, 37]. Caspase-1 plays a prominent role in the cleavage of pro-IL-1 β and pro-IL-18 to form mature IL-1 β and IL-18, respectively, which in turn play a pivotal role in the nitric oxide synthase (NOS) and cyclooxygenase-2 expression, as well as in the tumor necrosis factor-alpha (TNF- α) production (Fig. 3) [38, 39].

The activation of P2X7R is also involved in the generation of reactive oxygen species (ROS) in macrophages [39], microglia [40], and erythroid cells via the nicotinamide adenine dinucleotide phosphate (NADPH) oxidase 2 [41]. There is also evidence that P2X7R can enhance mitochondrial

ROS production via ATP [42, 43]. ROS contributes to inflammasome aggregation and IL-1 β release [44, 45].

Therefore, based on the P2X7R distribution in immune cells, the overexpression in inflammatory processes, and the activation of intracellular pathways leading to the release of pro-inflammatory cytokines, P2X7R has been proposed as one of the key players in inflammation [34].

P2X7R in chronic neurological disorders

As discussed above, P2X7R is expressed by several cell types in the Central Nervous System (CNS) and it is activated by massive release of ATP during acute harmful events such as mechanical damage, ischemia, status epilepticus, or in chronic neurodegenerative diseases, such as Alzheimer's Disease (AD), Parkinson Disease (PD), Multiple Sclerosis (MS), amyotrophic lateral sclerosis (ALS), and neuropathic pain. P2X7R activation is responsible for the release of neurodegeneration-inducing bioactive molecules such as pro-inflammatory cytokines, chemokines, proteases, reactive oxygen and nitrogen species, as well as the excitotoxic glutamate/ATP causing cellular damage.

The involvement of P2X7R in inflammatory responses in AD has been supported by several *in vitro* and *in vivo* studies. Microglial activation by β -amyloid (A β) requires P2X7R expression because A β -induced release of ATP and IL1- β was observed only in microglia from wild-type mice and not from P2X7R-deficient mice [46]. P2X7R overexpression induced by A β oligomers increased synaptic failure and neuronal dyshomeostasis in different cellular models of AD [47]. The overexpression of P2X7R has been confirmed in various animal models of AD [48] and in the brain of AD patients. In human AD brain, P2X7R is expressed in association with A β plaques and localized in immunoreactive microglia [49]. Finally, administration of the P2X7R antagonist Brilliant Blue G (BBG) in animal models of AD was able to reduce plaque loads in the hippocampus, neuroinflammatory response, and improve cognition [50].

P2X7R is also upregulated in PD patients' brains, contributing to excessive microglial activation and chronic neuroinflammation [51]. α -Synuclein binds to P2X7R in microglia and stimulates P2X7R transcription [52]. In the 6-OH-DOPA-lesioned rat model of PD, the administration of P2X7R antagonists BBG or A-438079 attenuates microgliosis and mitochondrial dysfunction, as well as motor and memory impairments [53, 54].

P2X7R plays different roles in ALS depending on the stage of the disease, being neuroprotective in the early stage, then progressing toward a neurodegenerative role in the middle and late stage [55].

In transgenic SOD1-G93A mice, the best-characterized animal model of ALS, the ablation of P2X7R induced more severe disease progression, increased gliosis, upregulation in inflammatory markers, and decreased motor neuron survival [40]. Moreover, in SOD1-G93A mice, the activation of P2X7R just before the onset of the pathological neuromuscular phenotype prevented denervation and atrophy of skeletal muscles and improved innervation and metabolism of myofibers [56].

P2X7R is upregulated on activated microglial cells in post-mortem spinal cord tissue of ALS patients [57], and high levels of extracellular ATP have been observed in cerebrospinal fluid samples from advanced ALS patients [58]. Activating P2X7R with benzoylbenzoyl ATP (BzATP), an ATP synthetic analogue, in SOD1-G93A mice microglia enhanced the oxidative stress with increased ROS production. These effects can be ameliorated by using the antagonists BBG, A-430879, and A-839977 [40]. Moreover, P2X7R activation initiated a neurotoxic phenotype in SOD1-G93A astrocytes, leading to motor neuron death in co-culture [59]. Finally, P2X7R contributed to ALS progression by modulating autophagic flux. Sustained P2X7R activation in SOD1-G93A microglia induced an increase in autophagy markers, and these effects could be ameliorated by using the antagonist A-804598 [60].

The involvement of P2X7R in MS is based on the observation that high expression levels of this receptor have been reported in activated microglia and astrocytes in the spinal cord and brain of MS patients [57]. P2X7R ablation suppressed the development of experimental autoimmune encephalomyelitis (EAE) in rats, which is considered a reliable model of MS. Consistently,

administration of BBG in EAE rats decreased astrogliosis and demyelination, leading to the amelioration of neurological symptoms [61]. Moreover, in EAE rats, the elevated expression of P2X7R in oligodendrocytes in normal-appearing axon tracts suggests that abnormalities in P2X7R expression are likely to precede the emergence of clinical symptoms and may be an early risk factor associated with early lesions formation in this disease [62].

P2X7R in autoimmune diseases

P2X7R is involved in innate and adaptive immunity. In innate immunity, the role of P2X7R is mainly related to the activation of the NLRP3/ASC/caspase-1 inflammasome and the production of pro-inflammatory cytokines. In adaptive immunity, P2X7R is involved in the proliferation and activation of T cells. In particular, activation of P2X7R inhibits the differentiation of T cells into regulatory T cells (Treg), an anti-inflammatory phenotype, and promotes the conversion of Treg in helper T cells (Th17), a pro-inflammatory phenotype. Dysregulation of innate and adaptive immune responses is responsible for autoimmune diseases such as inflammatory bowel disease (IBD), Crohn's Disease (CD), systemic lupus erythematosus (SLE), rheumatoid arthritis (RA), and systemic sclerosis (SSc) and, thus P2X7R antagonists can be helpful in the treatment of such diseases [63].

Elevated P2X7R levels in peripheral blood mononuclear cells and synovial fluid have been detected in RA patients and an arthritis rat model [64-66]. During the inflammation process in RA, several cytokine-independent pathways mediated by P2X7R are crucial, such as the P2X7R-cathepsin pathway. P2X7R antagonists AZ10573295 and AZ11648720 abolished the ATP-induced cathepsin release in macrophages from wild-type mice and the ATP-induced cathepsin release was not observed in macrophages from P2X7R^{-/-} [67].

The balance between Th17 and Treg cells regulated by P2X7R activation is a crucial pathogenic mechanism in IBD. In CD patients, besides the elevated expression of P2X7R, higher levels of IL-17 and lower levels of IL-10 were detected compared to controls, which were mainly produced by

Th17 and Treg cells, respectively [68]. In SSc, the activation of P2X7R could promote collagen production, α -smooth muscle actin expression, cell migration, and connective tissue growth factor release in LPS-primed fibroblasts from SSc patients, leading to pro-fibrotic effects. This effect was completely reversed by P2X7R antagonists or ERK1/2 inhibition, indicating a novel cytokine-independent pathway in P2X7R-induced fibrosis [69].

P2X7R in cancer

P2X7 is involved in the regulation of tumor cell growth in a complex manner. P2X7R is overexpressed in various malignancies, including pancreatic, breast, prostate, and colon cancers and neuroblastoma. Compared with normal tissue, the tumor microenvironment is characterized by higher ATP concentrations that activate P2X7R [30]. Therefore, depending on the intensity of ATP stimulation, P2X7R can promote cell growth or can induce cytotoxicity.

P2X7Rs promote cell growth under conditions of low-intensity ATP stimulation through modulation of mitochondrial metabolism and enhancing oxidative phosphorylation and aerobic glycolysis [70, 71]. In addition, P2X7R activates multiple intracellular growth-promoting pathways and it can also trigger a massive release of vascular endothelial growth factor (VEGF) [72], matrix metalloproteinases [73], or other tissue factors that promote tumor progression. In colorectal cancer cells, P2X7R activation promotes proliferation by activating the Akt and NF- κ B signaling pathways [74]. In pancreatic cancer cells, ATP-activated P2X7R promotes proliferation and growth through JNK and ERK1/2 signaling pathways [75]. In prostate cancer cells, P2X7R activation promotes invasion and metastasis by regulating the expression of epithelial-mesenchymal transition (EMT)-related genes and activating the PI3K/Akt and ERK1/2 signaling pathways [76]. Several studies have demonstrated that reducing P2X7R activity by using antagonists or negative allosteric modulators can reduce cancer cell growth and a number of preclinical studies have demonstrated that small-molecules antagonists [77] as well as anti-P2X7 antibodies [78] can be effective in the treatment of a variety of cancers. P2X7R induces cytotoxic effects when the stimulation with high

doses of ATP is associated with vacuolation, changes in membrane permeabilization, loss of mitochondrial potential, cell swelling, and an increase in mitochondrial Ca^{2+} [70]. High doses of ATP reduce the viability of acute myeloid leukemia cells through the activation of P2X7R but have no cytotoxic effect on normal hematopoietic stem cells [79]. In colon cancer cells, activation of P2X7R by extracellular ATP triggers apoptosis through the Akt/PRAS40/mTOR signaling pathway [80, 81]. In the GL261 glioma cell line, BzATP induces cell death and this effect is blocked by P2X7R antagonists [82].

4. P2X7R antagonists

Over the years, the search for selective P2X7 antagonists has been pursued by research groups from pharmaceutical companies and from academia. A variety of biological endpoints to monitor P2X7R function have been used, including measurement of channel activity using cation flux (usually calcium flux), exploitation of the pore-forming properties by measuring the uptake of fluorescent DNA binding dyes (ethidium bromide or Yo-Pro), and measurement of inflammatory readouts by monitoring the release of IL-1 β (the reader can find more details in ref. [1]). For clarity, the functional assay used to assess the activity of each class of compounds is detailed to allow a proper comparison of different antagonists.

The first generation of P2X7R antagonists represented by the Brilliant Blue G (BBG) [83] and the tyrosine derivative KN-62 [84] showed preferential activity at the rat and human P2X7R, respectively (Fig. 4) [85]. Although KN-62 is one of the most potent non-competitive antagonists for human P2X7R (hP2X7R), it is not suitable for therapeutic purpose because of the high molecular weight, high lipophilicity, and the presence of metabolically labile sulfonate groups. Therefore, the studies have been focused on the development of P2X7R antagonists characterized by high potency (hP2X7R pA_2 or $\text{pIC}_{50} > 7$), low molecular weight ($\text{MW} < 450$), acceptable lipophilicity ($\text{clogP} < 3.0$) with associated higher solubility, *in vitro* metabolic stability, bioavailability and *in vivo* good species cross-over (i.e., the same level of activity across species,

including humans). This latter aspect is particularly important because some series of P2X7R antagonists show poor species cross-over, making troublesome the translatability of the results from rodents to humans and vice versa. When available, the activity data at human P2X7R (hP2X7R) and rat P2X7R (rP2X7R) have been included to support the discussion of this relevant aspect.

Several second-generation antagonists, such as A-438079 [86], A-740003 [87], and GSK-314181A [88] (Fig. 4), are valuable pharmacological tools with suitable drug-like properties for *in vivo* studies. Their discovery marked the beginning of research efforts for the development of novel chemotypes as P2X7R antagonists [89, 90].

Mutagenesis and computer-aided docking studies indicated that A740003 and A438079 acted as P2X7R negative allosteric modulators. This was confirmed by the crystal structures of the complexes of the giant panda P2X7R bound to five structurally diverse compounds, including A740003, showing that the compounds were bound to a binding pocket distinct from the ATP binding pocket [91]. Karasawa et al. deposited five ligand-bound crystal structures of giant panda P2X7R with the compounds A-740003, A-804598, GW-791343, JNJ-47965567, and AZ-10606120 [26]. The crystal structures indicate that all the compounds, even though structurally diverse, interact with the same allosteric binding pocket, adopt similar orientations in the P2X7R allosteric site, and form contacts with a similar set of amino acids (Fig. 5). The compounds A-740003 (PDB code: 5u1u) and A-805498 (PDB code: 5u1v), which share similar chemical structures, are also characterized by similar ligand-protein contact patterns. In both cases, the quinoline moiety is oriented towards the upper side of the binding pocket, making interactions with the same set of residues, PHE88, MET105, PHE108, LYS110, and TRP167 (in the case of A-805498, quinoline also forms contact with ILE310, whereas for A-740003 this amino acid interacts with amino groups located in other parts of the molecule). The dimethoxy phenyl moiety of A-740003 makes contact with PHE95, PRO96, TYR295, and ALA296, whereas the phenyl ring of A-805498 interacts with TYR93, THR94, PHE95, PHE103, PHE293, and TYR295. In the ligand-receptor complex of compound GW-791343 (PDB code: 5u1y), 1-benzylpiperazine moiety contributes to a slightly

different location of the co-crystallized compound in the binding pocket. In fact, the piperazine ring interacts with SER85 and GLU305, whereas the benzyl moiety makes contacts with PHE88, PHE108, and LYS110. Acetamide and difluorophenyl moieties interact with the same amino acids as the respective parts of A-740003 and A-805498. As for JNJ-47965567, the crystal structure (PDB code: 5u1x) evidenced that the compound is located similarly to other compounds in the binding cavity, with the phenylsulfanylpyridine moiety sticking out of the binding pocket and the phenylpiperazine located deep in the pocket. Finally, AZ-10606120 (PDB code: 5u1w) is characterized by the highest structural diversity compared to the other compounds with the adamantyl and quinoline moieties in the same structure. The adamantyl moiety points to the deeper side of the pocket and forms contact with ALA91, TYR93, THR94, PHE95, PHE293, TYR295, and VAL312. On the other hand, the hydroxymethyl amino group occupies the upper region of the P2X7R binding site. Thus, the analysis of the crystal structures evidenced crucial interactions represented by a hydrogen-bonding donor group (amide or cyanoguanidine) forming contacts with ASP92 and two adjacent areas, one more lipophilic that points to the inner part of the receptor that accommodates adamantane or different phenyl rings, and one less lipophilic area pointing towards the extracellular side of the receptor that can accommodate more polar portions such as “pyridine-like” rings or the ethylenediamine substituent.

As several review articles on P2X7R antagonists have been published so far [92], in this manuscript, we analyze both patent and journal literature issued by 2010 dealing with medicinal chemistry efforts in the identification of P2X7R antagonists. An attempt is made to group structurally related compounds and to highlight common issues in the development of effective pharmacological tools or clinical candidates. The approaches adopted in the optimization process have been discussed.

Arylamides

This class of compounds originated from the adamantane amides first described by Astra Zeneca and it is exemplified by compound **1** (Fig. 6) [93]. Early examples of these compounds suffered from high lipophilicity and the consequent low aqueous solubility and poor metabolic stability [92]. The structure-activity relationship (SAR) studies evidenced the importance of an ortho-substituent (preferably -Cl) on the phenyl ring linked to the amide function, which causes a twist in the orientation of the benzamide that is necessary for potent P2X7R antagonism and of a lipophilic group linked to the amide function. Therefore, numerous potent arylamide-based P2X7R antagonists were developed by relying on these two pharmacophoric features.

Kassiou and colleagues explored the chemical space around compound **1** by replacing the adamantane nucleus with other polycycles, such as the cubane and different carboranes (compounds **2** and **3**, Fig. 7). *In vitro* data evidenced that the potency of such compounds was related to the dimensions of the lipophilic cage, i.e., the larger the cage, the higher the activity. However, larger lipophilic cages significantly contributed to the high lipophilicity of the compounds that were poorly bioavailable *in vivo*. In fact, only the compounds showing ligand-lipophilicity efficiency higher than 5 were active in animal models of depression [94]. To overcome the metabolic liability, the benzene ring of compound **1** was isosterically replaced with pyridine, pyrimidine, or pyridazine. This approach was unsuccessful because the azabenzamides were less potent than **1**. Therefore, the fluorine-for-hydrogen substitution on the adamantane cage was implemented as an alternative strategy to improve metabolic stability because the polar covalent C-F bond reduces lipophilicity and blocks metabolically sensitive sites. In addition, the small atomic radius of fluorine mimics the hydrogen atom, ensuring that no steric bulk is added to the molecule. The fluorinated derivatives showed antagonism at human P2X7R in the nanomolar range, suggesting that the fluorine-for-hydrogen substitution was well tolerated. In particular, the compound **4** (also known as SMW139, Fig. 7), featuring three fluorine atoms on the adamantane cage, showed the best combination of activity, *in vitro* metabolic stability, and *in vivo* bioavailability [95]. However, as already reported

for other adamantane amide derivatives [92], these fluorinated compounds showed poor cross-over, being less potent at mouse P2X7R (mP2X7R) than at human P2X7R.

Pfizer explored the 2-chlorobenzamide template starting from compound **5** (Table 1) [96], which showed potent hP2X7R antagonist activity, acceptable physicochemical properties, but low microsomal stability. The first structural modification was focused on the replacement of the metabolically liable methyl substituent on the pyridine ring with other substituents (OMe, CN, F, Cl), leading to compounds displaying a wide range of antagonist potency and metabolic stability. The best combination of properties was shown by compound **6** (Table 1), bearing a 5-fluoropyrimidyl ring, which also showed promising *in vivo* CNS exposure but a relatively short half-life (0.6 h). The carbocycle ring was identified as the main soft spot for metabolism; thus, it was further modified by reducing the size of the ring from seven to five methylene units. The size of the carbocycle had an effect on hP2X7R antagonism: the introduction of the cyclohexane ring gave a slight increase in metabolic stability but also a slight reduction of potency. Next, the fluorination of the cyclohexyl ring further improved metabolic stability leading to compound **7** (Table 1), which showed good hP2X7R antagonist potency, low clearance in human microsomes ($CL_{int} < 8.8$ mL/min/kg), and acceptable permeability ratio in MDCK cells. *In vivo* pharmacokinetic (PK) studies confirmed that the improved *in vitro* pharmacokinetic properties of compound **7** resulted in acceptable CNS exposure [97].

Pfizer developed another series of 2-chlorobenzamide derivatives starting from compound **8** (Fig. 8), bearing a 2-ethyl-1-hexyl chain as the lipophilic moiety. Compound **8** had moderate P2X7R antagonist activity in the IL-1 β assay ($IC_{50} = 0.8$ μ M), relatively low molecular weight but quite high lipophilicity. The first structural modification focused on the alkyl substituent linked to the amide function to improve potency and reduce lipophilicity. The SAR studies evidenced that the potency was related to the size of the alkyl substituent that had to fill properly the lipophilic pocket of the binding site, i.e., the same pocket region which was occupied by the adamantane nucleus in compound **1**. The replacement of the alkyl substituent with a benzyl group or a higher homolog led

to a complete loss of activity. The replacement of the 2-ethyl-1-hexyl chain with the 1-hydroxycycloheptyl substituent in compound **9** substantially improved potency ($IC_{50}= 0.083 \mu M$) and lipophilicity. In addition, compound **9** was predicted as a low-clearance compound in human liver microsomal and hepatocyte studies. Next, it was evidenced that the N3 proton of the 6-azauracil ring was not necessary for activity. Therefore, different substituents were linked at such a position. The introduction of the (R)-1-hydroxy-2-methoxyethyl group (compound **10**, also known as CE-224535, Fig. 8) provided the best combination of potency ($IC_{50}= 1.4 nM$) and lipophilicity, and *in vivo* PK properties in rats. However, like other benzamide derivatives, CE-224535 showed poor species cross-over. In addition, the 6-azauracil series was also characterized by low distribution volume (V_d) in dogs and monkey resulting in a short predicted half-life in humans [98]. Therefore, the 6-azauracil ring was replaced with different azolyl or azinyl rings leading to the identification of several potent hP2X7R antagonists with a wide range of metabolic stability (compounds **11-13**, Fig. 9). Compound **12** showed the best combination of potency and microsomal stability, but poor species cross-over. Therefore, this class of compounds was not further developed [99]. The 6-azauracil derivative CE-224535 (Fig. 8) was progressed to a phase II clinical trial (NCT00628095) to assess efficacy and safety in patients with active rheumatoid arthritis and inadequate response to methotrexate. CE-224535 was not as efficacious as compared to placebo even though it demonstrated acceptable safety and tolerability profile [100].

AstraZeneca filed two patent applications covering arylamide derivatives [101, 102], the most potent compounds being **14** and **15** (Fig. 10) with pIC_{50} values of 8.4 and 8.1, respectively, in THP-1 cells. In this series, the arylamide moiety is a quinoline-5-carboxamide nucleus bearing a chlorine at 6-position that mimics the chlorine in *ortho*-position of benzamide **1**, and an hydroxycycloalkane as the lipophilic moiety. The quinoline ring was substituted in 2-position with polar groups, reducing the lipophilicity and improving PK properties.

Starting from the antagonists **14** and **15**, Xiao et al. further explored the 6-chloroquinoline-5-carboxamide motif by introducing structural diversity at 2-position of the quinoline ring and the

lipophilic substituent linked to amide function [103]. The SAR analysis confirmed that the 2-position of the quinoline ring tolerated a wide range of substituents. In fact, the introduction of polar side chains or heterocycles increased potency compared to the unsubstituted counterpart (see **16** and **17** vs. **18**, Table 2). However, the compounds showed low metabolic stability, low cell permeability, and a high efflux ratio (compound **18**). To improve such properties, the basic moieties introduced in the 2-position were substituted with fluorine atoms or, as an alternative, the number of hydrogen bond donors in the 2-substituent was reduced (compound **19**, Table 2). Compound **19** (Table 2) showed the best combination of potency at hP2X7R, low liver microsomal clearance, and efflux ratio. However, compound **19** showed poor species cross-over that was not improved by the structural modifications performed on the cyclohexane ring (compounds **20-22**), thus limiting the possibility of further developing this class of compounds [103].

Using a high-throughput screening (HTS) approach, Janssen identified the N-(cyclohexylmethyl)benzamide as a scaffold to deliver P2X7R antagonists, in which the cyclohexylmethyl moiety represents the lipophilic moiety required for interaction with the hydrophobic pocket of the binding site. The most promising compounds were the 2-methyl-N-1,2,3,4-tetrahydroisoquinoline JNJ-42253432 (compound **23**, Fig.11) and the 2-(phenylthio)-nicotinamide JNJ-47965567 (compound **24**, Fig. 11) [104]. Both compounds were potent antagonists at hP2X7R and rP2X7R, able to penetrate into CNS and occupy rP2X7R after subcutaneous administration. Despite the promising activity profile, both compounds were not developed further because of the lack of selectivity towards other biological targets, such as serotonin and dopamine transporters. In addition, high metabolic liability made these compounds not suitable for oral administration [104].

Lundbeck disclosed two series of *ortho*-substituted benzamides (Table 3 and 4) in which the lipophilic adamantane nucleus of compound **1** was replaced by an arylcycloalkyl moiety [105, 106]. Also, for these compounds, the presence of an *ortho*-Cl substituent on the benzamide ring was preferred for high antagonist potency (see compounds **25-29** in Table 3 and compound **30** in Table

4). Electron-withdrawing substituents, such as -F or -CF₃, were inserted on the cycloalkyl moieties to limit metabolic liability.

Researchers at Lundbeck investigated a series of 2-(pyrimidin-2-yl)-4-(trifluoromethyl)thiazole-5-carboxamides (Fig. 12) loosely resembling the P2X7R antagonists listed in Table 4 [107]. The installation of a biphenyl-like system bearing the bulky CF₃ substituent close to the amide function provided high P2X7R antagonist potency, as in the case of racemic compound **33** (Fig. 12) [108].

The resolution of the enantiomers enabled the evaluation of the *S*-enantiomer, which was more potent than the *R*-enantiomer (IC₅₀= 12 nM and 89 nM, respectively) (Fig. 12). In addition, *S*-enantiomer provided a robust species cross-over (hP2X7 IC₅₀= 12 nM, rP2X7 IC₅₀= 2.2 nM, mP2X7 IC₅₀= 22 nM) [108]. *S*-**33** (also known as LuAF27139) had good oral bioavailability, CNS permeability, and no relevant safety issues. When orally administered in rats or mice, *S*-**33** reduced IL-1β release induced by intracerebroventricular administration of LPS [108].

The replacement of the lipophilic moiety linked to the amide group with a simple cycloalkane group has been also explored for quinoline carboxamide derivatives. Rech and coworkers reported a series of quinolinecarboxamides in which the amide function was linked to the 2-[2-(trifluoromethyl)pyrimidin-5-yl]ethyl group [109, 110]. SAR analysis evidenced that the 2-position of the quinoline moiety allowed the incorporation of a variety of functional groups (small alkyl, alkoxy, aliphatic rings) via an amine linkage giving a wide range of hP2X7R potency. In particular, compounds **34** and **35** (Table 5) had good potency at both human and mouse P2X7Rs. Notably, the chiral center in the substituent linked in the 2-position of the quinoline ring affected hP2X7R potency (compounds **34** and **35**, Table 5). Compound **34** was stable in mouse and human whole blood assay and attenuated the IL-1β release in both species. A tissue distribution study in the mouse showed that compound **34** had good peripheral bioavailability and rather good CNS exposure. Therefore, it was proposed as a tool to study the role of P2X7R in peripheral inflammation. However, in a mouse spared nerve injury model of tactile allodynia compound **34** did

not induce an effect on analgesic or anti-inflammatory response, suggesting that the blockade of peripheral P2X7R was not sufficient in this animal model of pain and inflammation [109, 110].

Rigidified arylamides

Several research groups have studied arylamides in which the amide function is completely or partially embedded in a cyclic system. The general formula of a large set of compounds is reported in Fig. 13. The SAR showed that the preferred substitution pattern on ring A was 2-Cl, 3-CF₃, or 2,3-diCl and that various Ar- were tolerated at ring D. The most sensitive part of the scaffold in terms of potency was ring B, in which the introduction of an alkyl substituent gives rise to a stereocenter that can greatly affect compound activity. On ring C, the topology of one or more aza groups influences the potency and species cross-over.

GlaxoSmithKline (GSK) disclosed in a patent application more than two hundred 5,6,7,8-tetrahydro-[1,2,4]triazolo[4,3-*a*]pyrazines as antagonists at hP2X7R. The SARs evidenced that the substitution pattern of the benzamide ring was important for antagonist potency, being the 2-Cl,3-CF₃-substitution preferred. In addition, the presence of an aromatic substituent in 3-position of the triazolopyrazinyl nucleus improves potency (Table 6) [111].

Janssen Pharmaceutical further evaluated compound **48** and confirmed potent antagonist activity at hP2X7R but found low potency at rP2X7R (compound **49**, Table 7) [112]. Compounds **51** and **52**, that are analogs of **49**, also showed this characteristics. Therefore, the pyrazine core (ring B, Fig. 13) was decorated with a methyl group to investigate if this structural modification affected amide bond conformation and possibly improved potency and species cross-over. The introduction of methyl in 5-, 6-, or 8-position of the triazole-pyrazine core of compound **52** led to compounds **53-55**, respectively (Table 7). This structural modification was well tolerated with respect to hP2X7R potency, also leading to a 40-fold gain in potency at rP2X7R in the case of 6-methyl derivative compound **54**. Considering the importance of species cross-over, the authors investigated the effect of stereochemistry in various 6-methyl derivatives, exemplified by compound **56**, whose *S*-

enantiomer was 200-fold more potent than the *R*-enantiomer at hP2X7R and did not show species cross-over being equipotent at rP2X7R (Table 7). Various optically active 6-methyl derivatives were investigated, including compound *S*-**54** and compound **57** (JNJ-54173717) showing high potency at both human and rat P2X7R [112].

In addition, JNJ-54173717 was labeled with ¹¹C for developing a PET radiotracer to assess the potential of P2X7R antagonism in preclinical models of CNS disorders (see PET radioligands Paragraph).

Continuing the investigation of the 1,2,4-triazolopyrazine core, it was found that when a phenyl was introduced in 8-position, functionalities as small as H in 3-position could provide excellent activity at hP2X7R but very low at rP2X7R activity (compound **58**, Table 8) [113]. The introduction of a larger substituent in 3-position, such as cyclopropyl, increased potency at rP2X7R (compound **59**, Table 8). However, these compounds were P-glycoprotein (Pgp) substrates, probably because of the relative basicity of the triazole ring. Thus, electron-withdrawing substituents were introduced to reduce basicity, as in the case of 3-CF₃ derivative **62** (Table 8), which was characterized by an efflux ratio below 2, good *in vivo* PK properties, and high receptor occupancy in autoradiography studies [113].

Janssen Pharmaceuticals further explored ring B and ring C (Fig. 13), targeting the 1,2,3-triazolopiperidine core (Table 9), as in the case of compound **63** that had nanomolar activity at hP2X7R but 700-fold lower potency at rP2X7R [114]. In addition, compound **63** was rapidly metabolized by human and rat microsomes. In an attempt to improve metabolic stability, the authors designed compounds characterized by lower lipophilicity. Thus, the N-1 phenyl substituent was replaced with several heteroaromatic rings, and this left the activity at hP2X7R unchanged, while significantly improving potency at rP2X7R (compounds **64** and **65**, Table 9). This structural modification also contributed to improving metabolic stability. The optimization of the substitution pattern of the benzamide ring evidenced that 2,3-disubstitution was preferred, for the 2-Cl,3-CF₃ derivative **66**, and the 2,3-diCl derivative **67** (Table 9). However, the *in vivo* PK properties were

quite poor [114]. In a subsequent paper, the effect of the introduction of a methyl substituent on the piperidine ring was explored. It was found that this structural modification led to an improvement of pharmacokinetic properties and CNS partitioning of the molecule and that the preferred configuration at chiral carbon was *R*. Among the studied compounds, JNJ-54175446 (Fig.14) was selected as clinical candidate and is currently under investigation for the treatment of major depressive disorders (NCT 04116606) [115].

An additional modification of ring B and ring C (Fig. 13) is represented by the compounds listed in Table 10, featuring an imidazopyridine core [116]. This replacement left the activity at human receptor unchanged, but it was detrimental to activity at rP2X7R ($IC_{50} > 500$ nM) and metabolic stability as well (compare compounds **50** and **51**, Table 7 vs. compounds **68** and **69**, Table 10). Next, the same strategy for the 1,2,4-triazolopyrazine derivatives was applied, i.e., a methyl was introduced in 4-position of the imidazopyridine core. This structural modification significantly improved metabolic stability but had little or no effect on rP2X7R activity (compounds **70** and **71**, Table 10). Compounds *R*-**71** and *R*-**72** (Table 10) were active at both human and rat P2X7R, metabolically stable, and did not block CYP450 or hERG. Compound *R*-**71** (JNJ-54166060) showed high oral bioavailability ($F > 50\%$) in rats and a percentage of receptor occupancy in agreement with the IC_{50} value *in vitro* [116].

A subsequent study evaluated a set of pyrido-pyrimidines that might be considered higher homologs of the previously presented imidazopyridines (compounds **73** and **74**, Fig. 15) [117]. This structural modification had little effect on hP2X7R activity but greatly reduced rP2X7R activity. Yet, the good metabolic stability of these compounds made them worthy of further investigation. The first structural modifications were oriented at lowering lipophilicity by replacing the phenyl ring in 4-position with heteroaromatic rings (Table 11). Only compound **75** (Table 11) showed an acceptable overall profile with an improvement of both rP2X7R activity and metabolic stability. As observed in the other series of rigidified benzamides discussed above, the introduction of a methyl substituent close to amide nitrogen (6-position) provided a substantial improvement of rP2X7R activity while

maintaining hP2X7R potency and metabolic stability (compound **77**, Table 11). The optimization of the substitution pattern of the benzamide ring evidenced that the 2-F-4-Cl-disubstitution led to potent hP2X7R and rP2X7R antagonists, as in the case of compound **78** (Table 11). This set of benzamides showed high bioavailability ($F > 80\%$) and high brain receptor occupancy after oral administration [117].

Researchers at Janssen also evaluated the shifting of the carbonyl function of the amide bond, as can be seen comparing compounds **50** and **79** (Fig.16), thus obtaining a series of N-benzyl lactam derivatives (Table 12) [118]. Actually, the formal shift of the carbonyl function caused a loss of activity but the introduction of a methyl in 6-position of the triazolo-pyrazine (compounds **80**, Fig. 16) led to a >100-fold improvement in potency for both human and rat P2X7R.

Separation of the enantiomers of compound **80** led to the *S*-enantiomer compound *S*-**80** (Table 12), which was more potent than the *R*-enantiomer. The exploration of the substituent pattern of the benzyl ring showed that the 2-Cl,3-CF₃-disubstitution was preferred to obtain potent P2X7R antagonists. Variation of the substituent linked to 3-position of the triazole ring indicated that 5- or 6-membered heteroaromatic rings were well tolerated yet led to a slight loss of potency at rP2X7R (compounds *S*-**80**-*S*-**83**, Table 12). This series was characterized by good metabolic stability and acceptable water solubility, even though several compounds were P-gp substrates. Compound *S*-**80**, which had suitable efflux ratio in Caco-2 cells, was further evaluated *in vivo*, demonstrating high receptor occupancy in rat brain after oral administration [118]. Compound *S*-**83** was radiolabeled with tritium, leading to [³H]JNJ-54232334 (Fig. 17), a valuable radioligand for labeling P2X7R in brain with high degree specific binding in rat hippocampus [118].

Many research studies focused their attention on the substitution of the amine function or the phenyl ring of the benzamide with a bioisostere. Abbot covered a series of compounds where a tetrazole core replaced the amide function [119] and a series with a triazole core [120] already discussed by Guile and coworkers [92]. Fig. 18 shows the tetrazole derivative **84** (A-438079) and the triazole derivative **85**, both with nociceptive activity in a rat model of neuropathic pain.

La Roche developed a series of retroamides as P2X7R antagonists [121]. This class of compounds originated from the 1,4-dihydropyridinone derivative **86** (Fig. 19), identified by an HTS campaign, which had good antagonist potency at hP2X7R (IC_{50} = 104 nM) and high metabolic liability. Thus, the insertion of an additional nitrogen led to the corresponding ureas, exemplified by compounds **87-89** (Fig. 18) characterized by higher hP2X7R antagonist potency as compared to **86** and improved metabolic stability [121]. Further profiling of the urea derivatives evidenced low stability of the urea function in human plasma and the formation of glutathione (GSH) adducts, suggesting potential safety issues. Therefore, the urea linkage was modified and the 1,4-dihydropyridinone core was modified to a 1,2-dihydropyridinone system (compound **90**, Fig. 19). This structural modification proved to be successful because compound **90** maintained the P2X7R potency, it was stable in human and rat plasma and the GSH adducts formation was very low. Interestingly, position 5' of the scaffold could accept a variety of substituents allowing the modulation of physicochemical properties. The 1,2-dihydropyridinone derivatives were also potent at inhibiting the release of IL-1 β in a human whole blood assay. However, most of the 1,2-dihydropyridinone derivatives were positive for the Ames test because of the formation of the corresponding anilines. To overcome this issue, fluorine was inserted in the aniline ring (compound **91**, Fig. 19), obtaining compounds with reduced mutagenic activity and retained potency against hP2X7R. Unfortunately, the 1,2-dihydropyridinone derivatives showed poor species cross-over, and, thus, any further development was discontinued. When these compounds were tested *in vivo* in rat the activity was lost as previously reported for 1,2-dihydropyridinone derivative [121].

Aliphatic amides

GSK identified through a HTS 122screening campaign the compound **92** as a valuable starting point for its good *in vitro* potency (hP2X7R pIC_{50} = 7.4; rP2X7R pIC_{50} = 7.0) [122, 123]. The SAR studies evidenced that a di-substitution pattern on the benzyl moiety was preferred over monosubstitution or no substitution. In particular, 2,3- and 2,4-disubstitution led to an improvement

of hP2X7R potency. Structural modification of the amide linker evidenced that the secondary amide was preferred over tertiary amide or bioisosteric replacement with heterocycles, suggesting that the presence of an H-bond acceptor was pivotal for the interaction with the receptor. Similarly, replacing the pyrazole ring with other 5-membered heterocycles was not tolerated, except for the imidazole ring. The substitution of the phenyl ring linked to pyrazole with an electron-withdrawing group improved the metabolic stability. The removal of the phenyl ring led to a substantial increase in hP2X7R potency and metabolic stability (compound **93**, Fig. 20) [124].

Compound **93** was then selected for further optimization of the biological profile. The substitution pattern of benzyl moiety was explored, confirming that 2,3- and 2,4-disubstitution was preferred. In particular, the 2,4-dichloro and 2-Cl-3-CF₃- derivatives (compounds **94** and **95**, Table 13) exhibited hP2X7R potency in the nanomolar range.

The manipulation of the pyrazole ring had a different impact on antagonist potency (compounds **96-98**, Table 13). The replacement of methyl groups with alkyl substituents larger than ethyl was not tolerated as well as the isomeric replacement of the pyrazole ring. Only the insertion of a CF₃ on the pyrazole ring led to an improvement of the antagonist potency. However, these structural modifications increased the lipophilicity with a consequent reduction of the metabolic stability of the compound [125]. Compound **94**, which showed the best potency, metabolic stability, and solubility, was then progressed to *in vivo* studies. The compound showed acceptable *in vivo* PK properties and anti-hyperalgesic effects in a model of inflammatory pain [125]. A subsequent study investigated the replacement of the pyrazole with an imidazole. The SARs paralleled those observed in the pyrazole series. The N-methyl group of the imidazole ring had a major impact on rP2X7R potency as increasing the dimension of this substituent was detrimental to antagonist potency. Compound **99** (Fig. 21) showed the best combination of potency, selectivity, and PK properties [126].

In vivo studies evidenced that compound **94** is prone to time-dependently inhibit CYP3A4 isozyme due to the oxidation of the methyl substituents. Considering the pivotal role of pyrazole methyl

groups in the interaction with P2X7R, alternative classes of P2X7R antagonists were searched. HTS screening led to the identification of compound **100**, which shared some pharmacophore features with compound **94** [127]. The superimposition of the two molecules indicated that the carbonyl oxygens of the acyclic amide groups as well as the pyrazole nitrogen and the oxygen atom of the carbonyl in the pyridone ring, respectively, could interact with the same putative H-bond donor feature of the P2X7R. Thus, using a fingerprint-based similarity search based on compounds **94** and **100** and applying the filter of at least two H-bond acceptors, which should be present in the compound structure, the virtual screening campaign led to the identification of pyrrolidinone **101** as a new potential hit (Fig. 22) [127].

The exploration of the SARs on the pyrrolidinone moiety of compound **101** evidenced that: i) the (S)-enantiomer was the most active enantiomer (compound *S*-**101**, Table 14); ii) the replacement of N-isopropyl substituent with smaller alkyl groups was beneficial for P2X7R potency (compounds **102** and **103**, Table 14); iii) the removal of the cyclic carbonyl group led the loss of activity (compounds **104**, Table 14); iv) expanding the 5-membered ring to a 6-membered ring was tolerated (compounds **105**, Table 14) [128]. As for the substitution pattern of the benzyl ring, it was once more noted that 2,3- or 2,4-disubstitution were preferred, being the 2-Cl-3-CF₃- and the 2,4-diCl derivatives the most potent compounds (compounds **106** and **107**, Table 14). The combination of such structural features led to compound **108**, also known as GSK-1482160, that exhibited nanomolar activity at hP2X7R and acceptable activity at rP2X7R (pIC₅₀= 6.5), good *in vitro* and *in vivo* PK properties, including brain penetration. GSK-1482160 also had good efficacy in animal models of inflammatory and neuropathic pain [127]. Based on the results of preclinical studies, GSK-1482160 was progressed to a first-in-human study to assess the pharmacokinetics, pharmacodynamics, safety, and tolerability in healthy subjects. The effect of increasing doses (up to 1 g) of GSK-1482160 on ex-vivo IL-1 β production in blood was selected as PK/PD model to assess the efficacy of the compounds. Although the compound did not show relevant safety or tolerability issues, the dose regimen required to achieve the desired level of IL-1 β inhibition (> 90%) was not

compatible with the safety margin in a steady-state model. Therefore, GSK-1482160 was not further studied [128].

The main limitation of GSK-1482160 was the short *in vivo* half-life in dogs and monkey and, thus, possibly in humans. Therefore, the molecular scaffold of GSK-1482160 was further modified to block the most vulnerable sites of metabolism, i.e., the carbon atoms of the pyrrolidinone ring and, especially, the position adjacent to the carbonyl function (compounds **109-114**, Table 15) [129, 130]. The best result in terms of both hP2X7R activity and intrinsic clearance in rat microsomes was obtained when the α -carbon was replaced by a methylated nitrogen (compound **109**). On the other hand, difluorination of the α -carbon (compound **110**) or replacement with oxygen (compound **111**) increased the intrinsic clearance in rat microsomes suggesting the involvement of alternative metabolic routes. Replacement of the methyl group with larger substituents featuring a basic group, such as the ethylmorpholino (compound **114**), did not improve P2X7R potency and had a negative effect on P-gp interaction. On the other hand, the removal of the methyl group provided the potent P2X7R antagonist **112**. Compound **115** (Fig. 23) emerged as the front runner in this series due to the selectivity profile, the high exposure after oral administration, and the excellent efficacy in animal models of chronic inflammatory pain [129, 130].

Other structures

Cyanoguanidines analogues

The potent and selective cyanoguanidine P2X7R antagonist A-740003 (hP2X7 IC_{50} = 44 nM; rP2X7 IC_{50} = 18 nM, Fig. 4) developed by Abbot Laboratories provided an attractive starting point for the design of novel agents [97]. A subsequent study described a series of more lipophilic cyanoguanidine piperazines, exemplified by compounds **116** and **117** (Fig. 24) [131, 132]. The cyanoguanidine piperazines showed good activity and good species cross-over, but poor physicochemical properties. More recently, Patberg and colleagues bioisosterically replaced the cyanoguanidine linker of compound **116** with bioisosteres such as the squaric acid diamide that can

form the H-bond interactions required for P2X7R interaction. Compound **118** showed acceptable activity at hP2X7R ($pIC_{50}= 6.65$) but poor overall solubility. Therefore, the phenyl ring linked to the piperazine ring was removed with the aim of improving molecular flexibility and, consequently, solubility, leading to a marginal loss of potency (compound **119**, $pIC_{50}= 6.52$, Fig. 23). The optimization of the aromatic moiety linked to the squaric amide and the substitution pattern of the carbamoyl aromatic ring led to the identification of compound **120** (Fig. 24), which showed hP2X7R activity ($pIC_{50}= 7.62$) in the same range as compound **116**, acceptable solubility and metabolic stability [133].

The group of Kassiou also reported a series of adamantyl cyanoguanidines developed starting from compound A-804598 (Fig. 25), a truncated analog of A-740003, having potent P2X7R antagonist activity in calcium flux, IL-1 β release, and dye uptake assays. The design of the compounds relied on incorporating the adamantane core as the hydrophobic portion of the molecule connected to variously substituted aryl rings through the cyanoguanidine linker, as in compound **121** (Fig. 25) [134]. The SARs emerging from the data in Table 16 evidenced that the presence of a methylene group (linker L₁) between the adamantane core and the cyanoguanidine moiety was pivotal for P2X7R activity (compounds **121-123**, Table 16). In contrast, the insertion of methylene as linker L₂ led to a decrease in activity. As for the substitution pattern of the phenyl ring, the 2-substitution was preferred when L₂ was absent (compounds **125** and **126**, Table 16), whereas the 4-substitution led to a reduction of P2X7R activity (compounds **127** and **128**, Table 16). The authors hypothesized that the high potency of the 2-substituted derivatives when L₂ was absent was due to a steric clash with the cyanoguanidine linker, leading to a twisted conformation of the aryl ring resembling the effect of the ortho-substitution observed in the 2-substituted benzamides derivatives. Consistently, when L₂ was a methylene group, the activity dropped by one order of magnitude (compound **129**, Table 16). A different trend was observed when the aromatic moiety was a pyridyl ring: the 2-pyridyl derivative **130** was inactive (L₂ was absent, Table 16), whereas the 3-pyridyl derivative **131** (Table 16) had activity in the nanomolar range. It was speculated that the formation of an intramolecular H

bond between the pyridine nitrogen and the cyanoguanidine moiety stabilized an inactive conformation of compound **130**. The 5-quinoline derivative, compound **132** (Table 16) was the most potent compound within the series. The increase in potency was explained considering the 5-quinoline moiety as a constrained conformation of the 3-pyridyl ring in compound **131**, resulting in a more favorable conformation in the binding site. The adamantyl cyanoguanides also had good physicochemical properties, and compound **131** was selected for *in vivo* evaluation because of more favorable value of lipophilic efficiency (LiPE= 3.68) than compound **132** (LiPE= 3.06). Compound **131** acted centrally as it produced an antidepressant phenotype in the forced swim test [134].

Purine derivatives

To develop P2X7R antagonists endowed with optimal blood-brain barrier (BBB) penetration Calzaferri and coworkers designed a series of compounds connecting a purine-like heterocycle with a halobenzene through a non-complex spacer (Table 17). The halobenzene substructure was selected because this moiety usually afforded potency and selectivity within the family of benzamide P2X7R antagonists. The purine-like heterocycles would be favorable for BBB penetration [135].

The SARs evidenced the combination when a purine scaffold/acetyl spacer led to a substantial inhibition (63% at 10 μ M) of dye uptake in hP2X7-HEK293 cells stimulated with 30 μ M BzATP (compounds **133**, **134**, and **138**, Table 17). An effective combination was theophylline ring/sulfonyl spacer (compounds **139**, Table 17). The lipophilicity of the substituents on the heterocycle ring impacted the antagonist potency as the polar substituents led to a substantial decrease in activity (compounds **136** and **137**, Table 17).

The most potent compounds **134** and **139** were further characterized. Both compounds reduced IL-1 β release in murine peritoneal macrophages stimulated with LPS, were selective against rat P2X1, P2X2, and P2X4 receptors, and showed acceptable permeability properties in parallel artificial membrane permeability assay (PAMPA) [135].

1,4-Naphthoquinones

Faria and coworkers developed a class of 1,4-naphthoquinone with the aim of identifying a new scaffold for P2X7R antagonists (Table 18) [136]. The potency of antagonist activity at P2X7R depended on the presence of a substituent in position 2 of the 1,4-naphthoquinone ring (R_3). When $R_3 = H$, the compound is devoid of activity, while when R_3 is iodine or phenyl, the activity is in the nanomolar range. Of note, the introduction of substituents on the phenyl ring of compound **143** causes a dramatic reduction of activity (compounds **144** and **145**). Molecular docking studies suggested that R_3 substituent can form π -stacking interaction with an aromatic residue of the binding site, which is important for the activity. The increase of substituent volume might hinder this interaction. Compounds **142** and **143** showed promising stability in mouse and human liver microsomes and inhibited dose-dependently the carrageenan-induced paw edema in mice [136]. A subsequent study described six 8-hydroxy-2-(1*H*-1,2,3-triazol-1-yl)-1,4-naphthoquinones, in which compounds **146** and **147** (Table 18) potently reduced P2X7R-mediated dye uptake and had good pharmacokinetic and toxicological profile but poor BBB penetration [137].

Pislyagin and coworkers developed a series of 1,4-naphthoquinone thioglycosides such as compounds **148** and **149** and the corresponding tetracyclic derivatives compounds **150** and **151**, respectively (Fig. 26) [138]. These compounds were tested for P2X7 activity (calcium influx assay and dye uptake assay), cytotoxicity, and neuroprotective activity in neuroblastoma N2a cells at different concentrations providing a nonlinear dose-dependent activity. The maximal effects were observed at 5 μM for Ca^{2+} efflux and at 10 μM for dye uptake. Compounds **148** and **150** were the most effective of the group.

KN-62 conformers

KN-62, a first generation P2X7R antagonist endowed with potent and specific antagonism of ATP-induced IL-1 β release and suppression of MAPK pathways, has served as a template for the

development of P2X7R antagonists. Park and colleagues have reported a series of 2,5-dioxoimidazolidine derivatives as rigid conformers of KN-62, developed by analyzing the low energy conformation of KN-62, which contains the backbone of L-tyrosine [139]. Once the distances between the hydroxy group, carboxyl group, and the α -nitrogen of the tyrosine backbone in the low-energy conformation of KN-62 were calculated, the 2,5-dioxoimidazolidine was identified as a constrained mimetic scaffold suitable for extensive decoration (Fig. 27). Compound **152** (Fig. 27) showed promising hP2X7R antagonist activity in dye uptake assay (IC_{50} = 1.97 μ M) and it was selected as the lead compound for further modifications. Removal of R₁ substituent and replacing the Boc group (R₂) with a benzoyl moiety was beneficial for the activity, thus suggesting that substitution on the piperidine nitrogen was pivotal for P2X7R antagonism (compound **158**, Table 19). A further variation of the nature of the substituent of the piperidine nitrogen evidenced that the presence of aliphatic hydrophobic groups was preferred over aromatic groups and that the presence of a carbonyl function between the piperidine nitrogen and the hydrophobic ring improved hP2X7R antagonism (compounds **154**, **156**, **157**, Table 19), confirming that the presence of an H-bond acceptor function favors the interaction with the binding site. The di-halo substituted benzoyl group linked to the piperidine nitrogen was also beneficial for antagonist activity (compounds **160-162**, Table 19). Compound **161** (hP2X7 IC_{50} = 70 nM) also displayed potent inhibitory activity in an *ex vivo* model of LTP-induced pain signaling in the spinal cord and significant anti-inflammatory activity in *in vivo* models of inflammatory pain [139].

In a subsequent paper, the 2,5-dioxoimidazolidine ring was expanded to a pyrimidine-2,4-dione to which piperazine was linked. The SARs evidenced that the presence of di-substituted benzoyl rings or polycycloalkylcarbonyl groups linked to N4 piperazine nitrogen led to potent hP2X7R antagonists, as in the case of compound **163** (hP2X7 IC_{50} = 27 nM, Fig. 28) [140].

Miscellaneous

Researchers at Merck identified compound **164** (Table 20) as a new lead compound through an HTS screening campaign [141]. The compound exhibited low micromolar activity towards human and rat P2X7R (hIC_{50} = 248 nM; rIC_{50} = 233 nM) and low potency on IL-1 β release in human whole blood assay (IC_{50} = 3372 nM). In addition, the PK of compound **164** was quite poor and not suitable for chronic administration. It was found that an isopropyl group at C-7 of **164** could effectively replace the spiroindane system and that the C-2 benzyl group could be replaced with a 4-fluorophenyl ring (compound **166**, Table 20). Keeping unchanged the substitutions at C-2 and C-7, the effect of other structural modifications was studied: the insertion of an electron donating group in 4-position of the N-1 benzyl ring was detrimental for activity (compound **167**), whereas the introduction of a 3,4-diF-benzyl substitution slightly improved the activity (compound **168**). When the phenyl ring in C-2 position (R_1) was replaced by a heteroaryl substituent (i.e., compound **169**) a substantial increase in activity was observed. Compound **169** displayed the best overall profile and it was evaluated in an osteoarthritis rat model and a chronic neuropathic pain model, capable of reducing inflammatory pain but not neuropathic pain *in vivo* [141].

Mahmood and coworkers designed a series of adamantane-1-carbonyl thiourea derivatives (Table 21) formally derived from the adamantane benzamide **1**, by varying the substituted aromatic ring. Most of the compounds were active at other P2XR, including P2X4R, P2X2R, and P2X5R. The most potent and selective P2X7R antagonists were the 2-chloro-3-pyridinyl **174** and the 8-quinolinyl **175**. No data on PK properties or activity in preclinical studies are available [142].

5. P2X7R PET radioligands

During the last decade, P2X7R has become an interesting molecular imaging target, considering the key role played in inflammation. P2X7R has been and it is still actively studied as a target for imaging of neuroinflammation. Advanced biomedical imaging techniques such as positron emission tomography (PET) provide a sensitive noninvasive imaging technique to study and quantify receptor and enzyme expression *in vivo*. The availability of a tracer labeled with positron emitting

radionuclides, such as carbon-11 (^{11}C) or fluorine-18 (^{18}F) able to bind a protein expressed during neuroinflammation would allow *in vivo* detection and quantification of neuroinflammation in the early stage of disease and could facilitate the development and evaluation of specific treatments [143]. The development of a successful PET radioligand for brain imaging requires the fulfillment of several requirements, including high affinity and selectivity for the target, suitable specific binding versus non-specific binding, high binding potential, ability to permeate the blood-brain barrier with low or negligible interaction with the efflux pumps [144].

P2X7R has been proposed as a target for *in vivo* imaging of neuroinflammation as an alternative to the translocator protein 18 kDa (TSPO) because TSPO radioligands have shown several limitations in terms of low receptor binding, high inter-subject variability of binding affinity, nonspecific binding in human brain due to TSPO polymorphism [145].

Following the above-discussed criteria, several P2X7R antagonists have been labeled with ^{11}C or ^{18}F and evaluated in different models of neurodegenerative disorders characterized by neuroinflammation.

The first P2X7R PET radioligands were the cyanoguanidine [^{11}C]A-740003 and the benzamide [^{11}C]SMW64-D16 (Fig. 29), which showed only marginal brain uptake in rodent models of inflammation despite the high *in vitro* affinity for the receptor [146]. Next, a series of fluorinated analogs of SMW64-D16 were designed to improve brain uptake and *in vivo* metabolic stability. [^{11}C]SMW139 (Fig. 29) showed high metabolic stability in rat plasma and brain uptake in a rat model overexpressing hP2X7R. However, autoradiography studies did not show a significant difference in binding of [^{11}C]SMW139 between post-mortem brain of AD patients and healthy individuals [147]. On the other hand, more interesting results were obtained in a first-in-human study, as [^{11}C]SMW139 demonstrated increased volume of distribution and binding potential in active relapsing remitting MS patients as compared to healthy individuals, thus suggesting that the radioligand can be used as a marker of neuroinflammation in MS [148].

Another ^{11}C -labeled P2X7R antagonist is [^{11}C]GSK1482160 (Fig. 29), with nanomolar affinity for hP2X7R in HEK293 cells stably transfected with the receptor ($K_d = 1.15$ nM). *In vivo* pharmacokinetics in LPS-treated mice showed that [^{11}C]GSK1482160 accumulated into the brain with higher uptake in LPS-treated mice as compared to vehicle-treated mice. The binding of the radioligand was blocked by an excess of unlabeled GSK1482160 [149]. Based on such promising data, [^{11}C]GSK1482160 was studied in non-human primates showing high retention and homogenous distribution in the brain. Moreover, in experimental autoimmune encephalomyelitis rats, a model of MS, [^{11}C]GSK1482160 uptake in the lumbar spinal cord strongly correlated with P2X7R expression, activation of microglia, and disease severity [150]. However, *in vivo* pharmacokinetics of [^{11}C]GSK1482160 in humans evidence the presence of only 2% of the injected dose in the brain [151]. Due to this relevant drawback, other potential PET radioligands were developed based on the scaffold of GSK1482160, exemplified by [^{11}C]IUR-1802 and [^{11}C]IUR-1803, that showed *in vitro* affinity comparable or even higher than [^{11}C]GSK1482160. No *in vivo* studies on these radioligands have been reported so far [152].

Janssen R&D and KU Luven have reported the radiosynthesis and biological characterization of [^{11}C]JNJ-54173717 (Fig.29). Preclinical evaluation evidenced that the radioligand bound hP2X7R and rP2X7R with nanomolar affinity and specifically accumulated in the brain with fast elimination kinetics, suggesting that the radioligand was suitable for quantifying P2X7R expression in the brain [153]. However, in a first-in-human study, [^{11}C]JNJ-54173717 did not show significant differences in the total volume of distribution between PD patients and healthy controls and, thus, it was not possible to assess the validity of [^{11}C]JNJ-54173717 as a marker of neuroinflammation in PD's [154].

The first reported P2X7R ^{18}F -radioligand was the cyanoguanidine [^{18}F]EFB (Fig. 30), which showed very low brain uptake in LPS-treated rats and, thus, was not developed further [155].

[^{18}F]JNJ-64413739 (Fig. 30) has been recently developed by Janssen R&D. Preclinical evaluation in LPS-treated rats and in non-human primates evidenced that the radioligand was able to

specifically label P2X7R in the brain. Moreover, in healthy human individuals, [¹⁸F]JNJ-64413739 was demonstrated to be useful in studying receptor occupancy [156, 157]. In a mice model of status epilepticus, [¹⁸F]JNJ-64413739 uptake strongly correlated with seizure severity during status epilepticus in brain structures such as cerebellum and ipsi- and contralateral cortex, hippocampus, striatum and thalamus. Elevated [¹⁸F]JNJ-64413739 uptake was also observed in brain sections from patients with temporal lobe epilepsy when compared to control, thus suggesting a correlation between P2X7R expression and seizure severity [158].

Finally, Fu et al. a potential P2X7R PET radioligand to image peripheral inflammation, namely [¹⁸F]-PTTP (Fig. 30) that showed nanomolar affinity for P2X7R *in vitro* and could specifically label the receptor in inflamed tissues [159].

6. Conclusions

Over the last decade, huge efforts have been made in the field of P2X7R that have led to the identification of new chemical classes of antagonists, increased understanding of receptor pharmacology, and reports about the therapeutic potential of P2X7R based on preclinical and clinical studies.

In the quest for small molecule antagonists, several chemical classes have been identified or disclosed and, among these, the amide series firstly disclosed by Astra Zeneca is the most prevalent. The studies of the structure-activity relationships have resulted in the identification of new derivatives having improved drug-like properties as compared to the early lead compounds. The high lipophilicity is a common feature in several potent P2X7R antagonists and the medicinal chemistry programs have been oriented towards the improvement of drug-like properties. This have led to the identification of promising clinical candidates that are currently investigated in clinical trials for the treatment of CNS disorders or effective PET radioligands that have allowed not only the imaging of P2X7R in neurodegenerative diseases but also the evaluation of drug target engagement.

An important aspect in the development of P2X7R antagonists is the poor species cross-over, which can greatly hamper the translability of the results from *in vitro* to *in vivo* studies and from preclinical to clinical studies. With this respect, improving the chemical diversity of P2X7R antagonists can offer the possibility to reduce the attrition in the development of effective P2X7R antagonists. High-throughput screening can provide a rich source of leads for this target and the availability of several crystal structures of ligand-receptor complex, which have allowed to define the nature of the allosteric binding site and the crucial interactions, can speed the identification of structurally diverse P2X7R antagonists.

While rheumatoid arthritis was the front-running indication in the first clinical studies with P2X7R antagonists, in the last years the interest has been shifting towards CNS disorders and cancer based on the encouraging results of preclinical studies highlighting a pivotal role of the receptor in these pathologies. Ongoing clinical studies will allow to understand the translability of these results. In fact, it is perplexing that a considerable number of available P2X7R antagonists failed to enter into clinical development.

We believe that several hurdles, such as a full comprehension of P2X7R in human pathologies, species differences or receptor polymorphism, still hamper the full exploitation of the therapeutic potential of P2X7R. Nonetheless, the availability of drug-like antagonists as well as a better understanding of P2X7R biology would contribute to overcome these limitations in the near future.

List of Abbreviations

A β : β -amyloid

AD: Alzheimer's Disease

ALS: amyotrophic lateral sclerosis

ATP: adenosine triphosphate

BBB: blood-brain barrier

BBG: Brilliant Blue G

CD: Crohn's Disease

CL_{int}: intrinsic clearance

CNS: Central Nervous System

EAE: experimental autoimmune encephalomyelitis

IBD: inflammatory bowel disease

HTS: high-throughput screening

MS: Multiple Sclerosis

NLRP3: NOD-, LRR- and Pyrin domain-containing Protein 3

PD: Parkinson Disease

PET: Positron Emission Tomography

P-gp: P-glycoprotein

PK: pharmacokinetic

RA: rheumatoid arthritis

SAR: structure-activity relationship

SSc: systemic sclerosis

TSPO: translocator protein 18 kDa

Conflict of interest

The authors declare no competing financial interest.

Acknowledgments

All authors have contributed to the preparation of the manuscript.

7. References

[1] North, R.A. Molecular physiology of P2X receptors. *Physiol. Rev.*, **2002**, 82 (4), 1013-1067.

- [2] Burnstock, G.; Kennedy, C. Is there a basis for distinguishing two types of P2-purinoceptor? *Gen. Pharmacol.*, **1985**, *16* (5), 433-440.
- [3] Mehta, N.; Kaur, M.; Singh, M.; Chand, S.; Vyas, B.; Silakari, P.; Bahia, M.S.; Silakari, O. Purinergic receptor P2X₇: a novel target for anti-inflammatory therapy. *Bioorg. Med. Chem.*, **2014**, *22* (1), 54-88.
- [4] Syed, N.H.; Kennedy, C. Pharmacology of P2X receptors. *WIREs Membr. Transp. Signal.*, **2012**, *1* (1), 16–30.
- [5] Oliveira-Giacomelli, Á.; Petiz, L.L.; Andrejew, R.; Turrini, N.; Silva, J.B.; Sack, U.; Ulrich, H. Role of P2X₇ Receptors in Immune Responses During Neurodegeneration. *Front. Cell. Neurosci.* **2021**, *15*, 662935.
- [6] Junger, W.G. Immune cell regulation by autocrine purinergic signalling. *Nat. Rev. Immunol.*, **2011**, *11* (3), 201-212.
- [7] Soto, F.; Garcia-Guzman, M.; Stühmer, W. Cloned ligand-gated channels activated by extracellular ATP (P2X Receptors). *Membrane Biol.*, **1997**, *160* (2), 91-100.
- [8] Coddou, C.; Yan, Z.; Obsil, T.; Huidobro-Toro, J.P.; Stojilkovic, S.S. Activation and regulation of purinergic P2X receptor channels. *Pharmacol. Rev.*, **2011**, *63* (3), 641-683.
- [9] Sluyter, R. The P2X₇ Receptor. *Adv. Exp. Med. Biol.*, **2017**, *1051*, 17-53.
- [10] Di Virgilio, F.; Dal Ben, D.; Sarti, A.C.; Giuliani, A.L.; Falzoni S. The P2X₇ receptor in infection and inflammation. *Immunity*, **2017**, *47* (1), 15-31.
- [11] Jiang, L.; Baldwin, J.M.; Roger, S.; Baldwin, S.A. Insights into the molecular mechanisms underlying mammalian P2X₇ receptor functions and contributions in diseases, revealed by structural modeling and single nucleotide polymorphisms. *Front. Pharmacol.*, **2013**, *4*, 55.
- [12] Roger, S.; Mei, Z.Z.; Baldwin, J.M.; Dong, L.; Bradley, H.; Baldwin, S.A.; Surprenant, A.; Jiang, L.H. Single nucleotide polymorphisms that were identified in affective mood disorders affect ATP-activated P2X₇ receptor functions. *J. Psychiatr. Res.*, **2010**, *44* (6), 347-55.

- [13] Fuller, S.J.; Stokes, L.; Skarratt, K.K.; Gu, B.J.; Wiley, J.S. Genetics of the P2X7 receptor and human disease. *Purinergic Signal.*, **2009**, *5* (2), 257-262.
- [14] Sperlágh, B.; Vizi, E.S.; Wirkner, K.; Illes, P. P2X7 receptors in the nervous system. *Prog. Neurobiol.*, **2006**, *78* (6), 327-346.
- [15] Lenertz, L.Y.; Gavala, M.L.; Zhu, Y.; Bertics, P.J. Transcriptional control mechanisms associated with the nucleotide receptor P2X7, a critical regulator of immunologic, osteogenic, and neurologic functions. *Immunol. Res.*, **2011**, *50* (1), 22-38.
- [16] Wiley, J.S.; Sluyter, R.; Gu, B.J.; Stokes, L.; Fuller, S.J. The human P2X7 receptor and its role in innate immunity. *Tissue Antigens*, **2011**, *78* (5), 321-332.
- [17] Torres, G.E.; Egan, T.M.; Voigt, M.M. Hetero-oligomeric assembly of P2X receptor subunits. Specificities exist with regard to possible partners. *J. Biol. Chem.*, **1999**, *274* (32), 6653-6659.
- [18] Nicke, A. Homotrimeric complexes are the dominant assembly state of native P2X7 subunits. *Biochem. Biophys. Res. Commun.*, **2008**, *377* (3), 803-808.
- [19] Kawate, T.; Michel, J.C.; Birdsong, W.T.; Gouaux, E. Crystal structure of the ATP-gated P2X(4) ion channel in the closed state. *Nature*, **2009**, *460* (7255), 592-598.
- [20] Habermacher, C.; Dunning, K.; Chataigneau, T.; Grutter T. Molecular structure and function of P2X receptors. *Neuropharmacology*, **2016**, *104*, 18-30.
- [21] McCarthy, A.E.; Yoshioka, C.; Mansoor, S.E. Full-Length P2X7 structures reveal how palmitoylation prevents channel desensitization. *Cell*, **2019**, *179* (3), 659-670.
- [22] Costa-Junior, H.M.; Marques-da-Silva, C.; Vieira, F.S.; Monção-Ribeiro, L.C.; Coutinho-Silva, R. Lipid metabolism modulation by the P2X7 receptor in the immune system and during the course of infection: new insights into the old view. *Purinergic Signal.*, **2011**, *7* (4), 381-92.
- [23] Bidula, S.M.; Cromer, B.A.; Walpole, S.; Angulo, J.; Stokes, L. Mapping a novel positive allosteric modulator binding site in the central vestibule region of human P2X7. *Sci. Rep.*, **2019**, *9* (1), 3231.

- [24] Bin Dayel, A.; Evans R. J.; Schmid R. Mapping the site of action of human P2X7 receptor antagonists AZ11645373, brilliant blue G, KN-62, calmidazolium, and ZINC58368839 to the intersubunit allosteric pocket. *Mol. Pharmacol.*, **2019**, *96* (3), 355-363.
- [25] Caseley, E.A.; Muench, S.P.; Baldwin, S.A.; Simmons, K.; Fishwick, C.W.; Jiang, L.H. Docking of competitive inhibitors to the P2X7 receptor family reveals key differences responsible for changes in response between rat and human. *Bioorg. Med. Chem. Lett.*, **2015**, *25* (16), 3164-3167.
- [26] Karasawa, A.; Kawate, T. Structural basis for subtype-specific inhibition of the P2X7 receptor. *Elife*, **2016**, *5*, e22153.
- [27] Surprenant, A.; Rassendren, F.; Kawashima, E.; North, R.A.; Buell, G. The cytolytic P2Z receptor for extracellular ATP identified as a P2X receptor (P2X7). *Science*, **1996**, *272* (5262), 735-738.
- [28] Wilhelm, K.; Ganesan, J.; Müller, T.; Dürr, C.; Grimm, M.; Beilhack, A.; Krempl, C.D.; Sorichter, S.; Gerlach, U.V.; Jüttner, E.; Zerweck, A.; Gärtner, F.; Pellegatti, P.; Di Virgilio, F.; Ferrari, D.; Kambham, N.; Fisch, P.; Finke, J.; Idzko, M.; Zeiser, R. Graft-versus-host disease is enhanced by extracellular ATP activating P2X7R. *Nat. Med.*, **2010**, *16* (12), 1434-1438.
- [29] Khakh, B.S.; North, R.A. P2X receptors as cell-surface ATP sensors in health and disease. *Nature*, **2006**, *442* (7102), 527-532.
- [30] Pellegatti, P.; Raffaghello, L.; Bianchi, G.; Piccardi, F.; Pistoia, V.; Di Virgilio, F. Increased level of extracellular ATP at tumor sites: in vivo imaging with plasma membrane luciferase. *PLoS One*, **2008**, *3* (7), e2599.
- [31] Eltzschig, H.K.; Sitkovsky, M.V.; Robson, S.C. Purinergic Signaling during Inflammation. *N. Engl. J. Med.*, **2012**, *367* (24), 2322-2333.
- [32] Rassendren, F.; Buell, G.N.; Virginio, C.; Collo, G.; North, R. A.; Surprenant, A. The permeabilizing ATP receptor, P2X7. Cloning and expression of a human cDNA. *J. Biol. Chem.*, **1997**, *272* (9), 5482-5486.

- [33] Chessell, I.P.; Simon, J.; Hibell, A.D.; Michel, A.D.; Barnard, E.A.; Humphrey, P.P.A. Cloning and functional characterisation of the mouse P2X7 receptor. *FEBS Lett.*, **1998**, *439* (1-2), 26-30.
- [34] Adinolfi, E.; Giuliani, A.L.; De Marchi, E.; Pegoraro, A.; Orioli, E.; Di Virgilio, F. The P2X7 receptor: a main player in inflammation. *Biochem Pharmacol.*, **2018**, *151*, 234-244.
- [35] Di Virgilio F. Purinergic signalling in the immune system. A brief update. *Purinergic Signal.*, **2007**, *3* (1-2), 1-3.
- [36] Jacob, F.; Novo, C.P.; Bachert, C.; Van Crombruggen, K. Purinergic signaling in inflammatory cells: P2 receptor expression, functional effects, and modulation of inflammatory responses. *Purinergic Signal.*, **2013**, *9* (3), 285-306.
- [37] Peng, K.; Liu, L.; Wei, D.; Lv, Y.; Wang, G.; Xiong, W.; Wang, X.; Altaf, A.; Wang, L.; He, D.; Wang, H.; Qu, P. P2X7R is involved in the progression of atherosclerosis by promoting NLRP3 inflammasome activation. *Int. J. Mol. Med.*, **2015**, *35* (5), 1179-1188.
- [38] Lister, M.F.; Sharkey, J.; Sawatzky, D.A.; Hodgkiss, J.P.; Davidson, D.J.; Rossi, A.G.; Finlayson, K. The role of the purinergic P2X7 receptor in inflammation. *J. Inflamm. (Lond.)*, **2007**, *4*, 5.
- [39] Lenertz, L.Y.; Gavala, M.L.; Hill, L.M.; Bertics, P.J. Cell signaling via the P2X(7) nucleotide receptor: linkage to ROS production, gene transcription, and receptor trafficking. *Purinergic Signal.*, **2009**, *5* (2), 175-187.
- [40] Apolloni, S.; Parisi, C.; Pesaresi, M.G.; Rossi, S.; Carri, M.T.; Cozzolino, M.; Volonté, C.; D'Ambrosi, N. The NADPH oxidase pathway is dysregulated by the P2X7 receptor in the SOD1-G93A microglia model of amyotrophic lateral sclerosis. *J. Immunol.*, **2013**, *190* (10), 5187-5195.
- [41] Wang, B.; Sluyter, R. P2X7 receptor activation induces reactive oxygen species formation in erythroid cells. *Purinergic Signal.*, **2013**, *9* (1), 101-112.
- [42] Gross, O.; Thomas, C.J.; Guarda, G.; Tschopp, J. The inflammasome: an integrated view. *Immunol. Rev.*, **2011**, *243* (1), 136-151.

- [43] Tschopp, J. Mitochondria: Sovereign of inflammation? *Eur. J. Immunol.*, **2011**, *41* (5), 1196-1202.
- [44] Hung, S.C.; Choi, C.H.; Said-Sadier, N.; Johnson, L.; Atanasova, K.R.; Sellami, H.; Yilmaz, Ö.; Ojcius, D.M. P2X4 assembles with P2X7 and pannexin-1 in gingival epithelial cells and modulates ATP-induced reactive oxygen species production and inflammasome activation. *PLoS One*, **2013**, *8* (7), e70210.
- [45] Minkiewicz, J.; de Rivero Vaccari, J.P.; Keane, R.W. Human astrocytes express a novel NLRP2 inflammasome. *Glia*, **2013**, *61* (7), 1113-1121.
- [46] Sanz, J.M.; Chiozzi, P.; Ferrari, D.; Colaianna, M.; Idzko, M.; Falzoni, S.; Fellin, R.; Trabace, L.; Di Virgilio, F. Activation of microglia by amyloid {beta} requires P2X7 receptor expression. *J. Immunol.*, **2009**, *182* (7), 4378-85.
- [47] Sáez-Orellana, F.; Fuentes-Fuentes, M.C.; Godoy, P.A.; Silva-Grecchi, T.; Panes, J.D.; Guzmán, L.; Yévenes, G.E.; Gavián, J.; Egan, T.M.; Aguayo, L.G.; Fuentealba, J. P2X receptor overexpression induced by soluble oligomers of amyloid beta peptide potentiates synaptic failure and neuronal dyshomeostasis in cellular models of Alzheimer's disease. *Neuropharmacology*, **2018**, *128*, 366-378.
- [48] Parvathenani, L.K.; Tertyshnikova, S.; Greco, C.R.; Roberts, S.B.; Robertson, B.; Posmantur, R. P2X7 mediates superoxide production in primary microglia and is up-regulated in a transgenic mouse model of Alzheimer's disease. *J. Biol. Chem.*, **2003**, *278* (15), 13309-13317.
- [49] McLarnon, J.G.; Ryu, J.K.; Walker, D.G.; Choi, H.B. Upregulated expression of purinergic P2X(7) receptor in Alzheimer disease and amyloid-beta peptide-treated microglia and in peptide-injected rat hippocampus. *J. Neuropathol. Exp. Neurol.*, **2006**, *65* (11), 1090-1097.
- [50] Ryu, J.K.; McLarnon, J.G. Block of purinergic P2X(7) receptor is neuroprotective in an animal model of Alzheimer's disease. *Neuroreport*, **2008**, *19* (17), 1715-1719.

- [51] Durrenberger, P.F.; Grünblatt, E.; Fernando, F.S.; Monoranu, C.M.; Evans, J.; Riederer, P.; Reynolds, R.; Dexter, D.T. Inflammatory pathways in Parkinson's Disease; a BNE microarray study. *Parkinsons Dis.*, **2012**, *2012*:214714.
- [52] Jiang, T.; Hoekstra, J.; Heng, X.; Kang, W.; Ding, J.; Liu, J.; Chen, S.; Zhang, J. P2X7 receptor is critical in α -synuclein--mediated microglial NADPH oxidase activation. *Neurobiol. Aging*, **2015**, *36* (7), 2304-2318.
- [53] Carmo, M.R.; Menezes, A.P.; Nunes, A.C.; Pliássova, A.; Rolo, A.P.; Palmeira, C.M.; Cunha, R.A.; Canas, P.M.; Andrade, G.M. The P2X7 receptor antagonist Brilliant Blue G attenuates contralateral rotations in a rat model of Parkinsonism through a combined control of synaptotoxicity, neurotoxicity and gliosis. *Neuropharmacology*, **2014**, *81*, 142-152.
- [54] Kumar, S.; Mishra, A.; Krishnamurthy, S. Purinergic antagonism prevents mitochondrial dysfunction and behavioral deficits associated with dopaminergic toxicity induced by 6-OHDA in rats. *Neurochem. Res.*, **2017**, *42* (12), 3414-3430.
- [55] Volonté, C.; Amadio, S.; Liguori, F.; Fabbriozio, P. Duality of P2X7 Receptor in Amyotrophic Lateral Sclerosis. *Front. Pharmacol.*, **2020**, *11*, 1148.
- [56] Fabbriozio, P.; Apolloni, S.; Bianchi, A.; Salvatori, I.; Valle, C.; Lanzuolo, C.; Bendotti, C.; Nardo, G.; Volonté, C. P2X7 activation enhances skeletal muscle metabolism and regeneration in SOD1G93A mouse model of amyotrophic lateral sclerosis. *Brain Pathol.*, **2020**, *30* (2), 272-282.
- [57] Yiangou, Y.; Facer, P.; Durrenberger, P.; Chessell, I.P.; Naylor, A.; Bountra, C.; Banati, R.R.; Anand, P. COX-2, CB2 and P2X7-immunoreactivities are increased in activated microglial cells/macrophages of multiple sclerosis and amyotrophic lateral sclerosis spinal cord. *BMC Neurol.*, **2006**, *6*, 12.
- [58] Nukui, T.; Matsui, A.; Niimi, H.; Sugimoto, T.; Hayashi, T.; Dougu, N.; Konishi, H.; Yamamoto, M.; Anada, R.; Matsuda, N.; Kitajima, I.; Nakatsuji, Y. Increased cerebrospinal fluid adenosine 5'-triphosphate in patients with amyotrophic lateral sclerosis. *BMC Neurol.*, **2021**, *21* (1), 255.

- [59] Gandelman, M.; Peluffo, H.; Beckman, J.S.; Cassina, P.; Barbeito, L. Extracellular ATP and the P2X7 receptor in astrocyte-mediated motor neuron death: implications for amyotrophic lateral sclerosis. *J. Neuroinflamm.*, **2010**, *7*, 33.
- [60] Fabbrizio, P.; Amadio, S.; Apolloni, S.; Volontè, C. P2X7 Receptor activation modulates autophagy in SOD1-G93A mouse microglia. *Front. Cell. Neurosci.*, **2017**, *11*, 249.
- [61] Matute, C.; Torre, I.; Pérez-Cerdá, F.; Pérez-Samartín, A.; Alberdi, E.; Etxebarria, E.; Arranz, A. M.; Ravid, R.; Rodríguez-Antigüedad, A.; Sánchez-Gómez, M.; Domercq, M. P2X(7) receptor blockade prevents ATP excitotoxicity in oligodendrocytes and ameliorates experimental autoimmune encephalomyelitis. *J. Neurosci.*, **2007**, *27* (35), 9525-9533.
- [62] Amadio, S.; Parisi, C.; Piras, E.; Fabbrizio, P.; Apolloni, S.; Montilli, C.; Luchetti, S.; Ruggieri, S.; Gasperini, C.; Laghi-Pasini, F.; Battistini, L.; Volonté, C. Modulation of P2X7 receptor during inflammation in multiple sclerosis. *Front. Immunol.*, **2017**, *8*, 1529.
- [63] Cai, X.; Yao, Y.; Teng, F.; Li, Y.; Wu, L.; Yan, W.; Lin, N. The role of P2X7 receptor in infection and metabolism: Based on inflammation and immunity. *Int. Immunopharmacol.*, **2021**, *101* (Pt A), 108297.
- [64] Portales-Cervantes, L.; Niño-Moreno, P.; Doníz-Padilla, L.; Baranda-Candido, L.; García-Hernández, M.; Salgado-Bustamante, M.; González-Amaro, R.; Portales-Pérez D. Expression and function of the P2X(7) purinergic receptor in patients with systemic lupus erythematosus and rheumatoid arthritis. *Hum. Immunol.*, **2010**, *71*, (8), 818-825.
- [65] Fan, Z.D.; Zhang, Y.Y.; Guo, Y.H.; Huang, N.; Ma, H.H.; Huang, H.; Yu, H.G. Involvement of P2X7 receptor signaling on regulating the differentiation of Th17 cells and type II collagen-induced arthritis in mice. *Sci Rep.*, **2016**, *6*, 35804.
- [66] McInnes, I.B.; Cruwys, S.; Bowers, K.; Braddock, M.; Targeting the P2X7 receptor in rheumatoid arthritis: biological rationale for P2X7 antagonism. *Clin. Exp. Rheumatol.*, **2014**, *32* (6), 878-882.

- [67] Lopez-Castejon, G.; Theaker, J.; Pelegrin, P.; Clifton, A.D.; Braddock, M.; Surprenant, A. P2X(7) receptor-mediated release of cathepsins from macrophages is a cytokine-independent mechanism potentially involved in joint diseases. *J. Immunol.*, **2010**, *185* (4), 2611-2629.
- [68] Neves, A.R.; Castelo-Branco, M.T.; Figliuolo, V.R.; Bernardazzi, C.; Buongusto, F.; Yoshimoto, A.; Nanini, H.F.; Coutinho, C.M.; Carneiro, A.J.; Coutinho-Silva, R.; de Souza, H.S. Overexpression of ATP-activated P2X7 receptors in the intestinal mucosa is implicated in the pathogenesis of Crohn's disease. *Inflamm. Bowel Dis.*, **2014**, *20* (3), 444-457.
- [69] Gentile, D.; Lazzerini, P.E.; Gamberucci, A.; Natale, M.; Selvi, E.; Vanni, F.; Ali, A.; Taddeucci, P.; Del-Ry, S.; Cabiati, M.; Della-Latta, V.; Abraham, D.J.; Morales, M.A.; Fulceri, R.; Laghi-Pasini, F.; Capecchi, P.L. Searching novel therapeutic targets for scleroderma: P2X7-receptor is up-regulated and promotes a fibrogenic phenotype in systemic sclerosis fibroblasts. *Front. Pharmacol.*, **2017**, *8*, 638.
- [70] Adinolfi, E.; Callegari, M.G.; Ferrari, D.; Bolognesi, C.; Minelli, M.; Wieckowski, M.R.; Pinton, P.; Rizzuto, R.; Di Virgilio, F. Basal activation of the P2X7 ATP receptor elevates mitochondrial calcium and potential, increases cellular ATP levels, and promotes serum-independent growth. *Mol. Biol. Cell.*, **2005**, *16* (7), 3260-3272.
- [71] Adinolfi, E.; Callegari, M.G.; Cirillo, M.; Pinton, P.; Giorgi, C.; Cavagna, D.; Rizzuto, R.; Di Virgilio, F. Expression of the P2X7 receptor increases the Ca²⁺ content of the endoplasmic reticulum, activates NFATc1, and protects from apoptosis. *J. Biol. Chem.*, **2009**, *284* (15), 10120-10128.
- [72] Hill, L.M.; Gavala, M.L.; Lenertz, L.Y.; Bertics, P.J. Extracellular ATP may contribute to tissue repair by rapidly stimulating purinergic receptor X7-dependent vascular endothelial growth factor release from primary human monocytes. *J. Immunol.*, **2010**, *185* (5), 3028-3034.
- [73] Gu, B.J.; Wiley, J.S. Rapid ATP-induced release of matrix metallo- proteinase 9 is mediated by the P2X7 receptor. *Blood*, **2006**, *107* (12), 4946-4953.

- [74] Qian, F.; Xiao, J.; Hu, B.; Sun, N.; Yin, W.; Zhu, J. High expression of P2X7R is an independent postoperative indicator of poor prognosis in colorectal cancer. *Hum. Pathol.*, **2017**, *64*, 61-68.
- [75] Choi, J.H.; Ji, Y.G.; Ko, J.J.; Cho, H.J.; Lee, D.H. Activating P2X7 receptors increases proliferation of human pancreatic cancer cells via ERK1/2 and JNK. *Pancreas*, **2018**, *47* (5), 643-651.
- [76] Qiu, Y.; Li, W.H.; Zhang, H.Q.; Liu, Y.; Tian, X.X.; Fang, W.G. P2X7 mediates ATP-driven invasiveness in prostate cancer cells. *PLoS One*, **2014**, *9* (12), e114371.
- [77] Lara, R.; Adinolfi, E.; Harwood, C.A.; Philpott, M.; Barden, J.A.; Di Virgilio, F.; McNulty, S. P2X7 in cancer: from molecular mechanisms to therapeutics. *Front. Pharmacol.*, **2020**, *11*, 793.
- [78] Danquah, W.; Meyer-Schwesinger, C.; Rissiek, B.; Pinto, C.; Serracant-Prat, A.; Amadi, M.; Iacenda, D.; Knop, J.H.; Hammel, A.; Bergmann, P.; Schwarz, N.; Assunção, J.; Rothier, W.; Haag, F.; Tolosa, E.; Bannas, P.; Boué-Grabot, E.; Magnus, T.; Laeremans, T.; Stortelers, C.; Koch-Nolte, F. Nanobodies that block gating of the P2X7 ion channel ameliorate inflammation. *Sci. Transl. Med.*, **2016**, *8* (366), 366ra162.
- [79] Salvestrini, V.; Orecchioni, S.; Talarico, G.; Reggiani, F.; Mazzetti, C.; Bertolini, F.; Orioli, E.; Adinolfi, E.; Di Virgilio, F.; Pezzi, A.; Cavo, M.; Lemoli, R.M.; Curti A. Extracellular ATP induces apoptosis through P2X7R activation in acute myeloid leukemia cells but not in normal hematopoietic stem cells. *Oncotarget*, **2017**, *8* (4), 5895-5908.
- [80] Souza, C.O.; Santoro, G.F.; Figliuolo, V.R.; Nanini, H.F.; de Souza, H.S.; Castelo-Branco, M.T.; Abalo, A.A.; Paiva, M.M.; Coutinho, C.M.; Coutinho-Silva, R. Extracellular ATP induces cell death in human intestinal epithelial cells. *Biochim. Biophys. Acta*, **2012**, *1820*(12), 1867-1878.
- [81] White, N.; Butler, P.E.; Burnstock, G. Human melanomas express functional P2X(7) receptors. *Cell. Tissue Res.*, **2005**, *321* (3), 411-418.

- [82] Tamajusuku, A.S.; Villodre, E.S.; Paulus, R.; Coutinho-Silva, R.; Battasstini, A.M.; Wink, M.R.; Lenz, G. Characterization of ATP-induced cell death in the GL261 mouse glioma. *J. Cell. Biochem.*, **2010**, *109* (5), 983-991.
- [83] Jiang, L.H.; Mackenzie, A.B.; North, R.A.; Surprenant, A. Brilliant blue G selectively blocks ATP-gated rat P2X(7) receptors. *Mol. Pharmacol.*, **2000**, *58* (1), 82-88.
- [84] Gargett, C.E.; Wiley, J.S. The isoquinoline derivative KN-62 a potent antagonist of the P2Z-receptor of human lymphocytes. *Br. J. Pharmacol.*, **1997**, *120* (8), 1483-1490.
- [85] Donnelly-Roberts, D.L.; Namovic, M.T.; Han, P.; Jarvis, M.F. Mammalian P2X7 receptor pharmacology: comparison of recombinant mouse, rat and human P2X7 receptors. *Br. J. Pharmacol.*, **2009**, *157* (7), 1203-1214.
- [86] McGaraughty, S.; Chu, K.L.; Namovic, M.T.; Donnelly-Roberts, D.L.; Harris, R.R.; Zhang, X.F.; Shieh, C.C.; Wismer, C.T.; Zhu, C.Z.; Gauvin, D.M.; Fabiyi, A.C.; Honore, P.; Gregg, R.J.; Kort, M.E.; Nelson, D.W.; Carroll, W.A.; Marsh, K.; Faltynek, C.R.; Jarvis, M.F. P2X7-related modulation of pathological nociception in rats. *Neuroscience*, **2007**, *146* (4), 1817-1828.
- [87] Honore, P.; Donnelly-Roberts, D.; Namovic, M.T.; Hsieh, G.; Zhu, C.Z.; Mikusa, J.P.; Hernandez, G.; Zhong, C.; Gauvin, D.M.; Chandran, P.; Harris, R.; Medrano, A.P.; Carroll, W.; Marsh, K.; Sullivan, J.P.; Faltynek, C.R.; Jarvis, M.F. A-740003 [N-(1-{{[(cyanoimino)(5-quinolinylamino) methyl]amino}-2,2-dimethylpropyl]-2-(3,4-dimethoxyphenyl)acetamide}], a novel and selective P2X7 receptor antagonist, dose-dependently reduces neuropathic pain in the rat. *J. Pharmacol. Exp. Ther.*, **2006**, *319* (3), 1376-85.
- [88] Broom, D.C.; Matson, D.J.; Bradshaw, E.; Buck, M.E.; Meade, R.; Coombs, S.; Matchett, M.; Ford, K.K.; Yu, W.; Yuan, J.; Sun, S.H.; Ochoa, R.; Krause, J.E.; Wustrow, D.J.; Cortright, D.N. Characterization of N-(adamantan-1-ylmethyl)-5-[(3R-amino-pyrrolidin-1-yl)methyl]-2-chloro-benzamide, a P2X7 antagonist in animal models of pain and inflammation. *J. Pharmacol. Exp. Ther.*, **2008**, *327* (3), 620-633.

- [89] Gum, R.J.; Wakefield, B.; Jarvis, M.F. P2X receptor antagonists for pain management: examination of binding and physicochemical properties. *Purinergic Signal*, 2012, 8(Suppl 1), 41-56.
- [90] Donnelly-Roberts, D.L.; Jarvis, M.F. Discovery of P2X7 receptor-selective antagonists offers new insights into P2X7 receptor function and indicates a role in chronic pain states. *Br. J. Pharmacol.*, **2007**, 151 (5), 571-579.
- [91] Allsopp, R.C.; Dayl, S.; Schmid, R.; Evans, R.J. Unique residues in the ATP gated human P2X7 receptor define a novel allosteric binding pocket for the selective antagonist AZ10606120. *Sci. Rep.*, **2017**, 7 (1), 725.
- [92] Guile, S.D.; Alcaraz, L.; Birkinshaw, T.N.; Bowers, K.C.; Ebden, M.R.; Furber, M.; Stocks, M.J. Antagonists of the P2X(7) receptor. From lead identification to drug development. *J. Med. Chem.*, **2009**, 52 (10), 3123-3141.
- [93] Baxter, A.; Bent, J.; Bowers, K.; Braddock, M.; Brough, S.; Fagura, M.; Lawson, M.; McNally, T.; Mortimore, M.; Robertson, M.; Weaver, R.; Webborn, P. Hit-to-Lead studies: the discovery of potent adamantane amide P2X7 receptor antagonists. *Bioorg. Med. Chem. Lett.*, **2003**, 13 (22), 4047-4050.
- [94] Wilkinson, S.M.; Gunosewoyo, H.; Barron, M.L.; Boucher, A.; McDonnell, M.; Turner, P. Morrison, D.E.; Bennett, M.R.; McGregor, I.S.; Rendina, L.M.; Kassiou, M. The first CNS-active carborane: A novel P2X7 receptor antagonist with antidepressant activity. *ACS Chem. Neurosci.*, **2014**, 5 (5), 335-339.
- [95] Wilkinson, S.M.; Barron, M.L.; O'Brien-Brown, J.; Janssen, B.; Stokes, L.; Werry, E.L.; Chishty, M. Skarratt, K.K.; Ong, J.A.; Hibbs, D.E.; Vugts, D.J.; Fuller, S.; Windhorst, A.D.; Kassiou, M. Pharmacological evaluation of novel bioisosteres of an adamantanyl benzamide P2X7 Receptor antagonist. *ACS Chem. Neurosci.*, **2017**, 8 (11), 2374-2380.
- [96] Dombroski, M.A.; Duplantier, A.J.; Subramanyam, C. Benzamide inhibitors of the P2X7 receptor. PCT Appl. N. WO 2004099146, November 18, 2004.

- [97] Chen, X.; Pierce, B.; Naing, W.; Grapperhaus, M.L.; Phillion, D.P. Discovery of 2-chloro-N-((4,4-difluoro-1-hydroxycyclohexyl)methyl)-5-(5-fluoropyrimidin-2-yl)benzamide as a potent and CNS penetrable P2X₇ receptor antagonist. *Bioorg. Med. Chem. Lett.*, **2010**, 20 (10), 3107-3111.
- [98] Duplantier, A.J.; Dombroski, M.A.; Subramanyam, C. Beaulieu, A.M.; Chang, S.P.; Gabel, C.A.; Jordan, C.; Kalgutkar, A.S.; Kraus, K.G.; Labasi, J.M.; Mussari, C.; Perregaux, D.G.; Shepard, R.; Taylor, T.J.; Trevena, K.A.; Whitney-Pickett, C.; Yoon, K. Optimization of the physicochemical and pharmacokinetic attributes in a 6-azauracil series of P2X₇ receptor antagonists leading to the discovery of the clinical candidate CE-224,535. *Bioorg. Med. Chem. Lett.*, **2011**, 21 (12), 3708-3711.
- [99] Subramanyam, C.; Duplantier, A.J.; Dombroski, M.A.; Chang, S.P.; Gabel, C.A.; Whitney-Pickett, C.; Perregaux, D.G.; Labasi, J.M.; Yoon, K.; Shepard, R.M.; Fisher, M. Discovery, synthesis and SAR of azinyl- and azolylbenzamides antagonists of the P2X₇ receptor. *Bioorg. Med. Chem. Lett.*, **2011**, 21 (18), 5475-5479.
- [100] Stock, T.C.; Bloom, B.J.; Wei, N.; Ishaq, S.; Park, W.; Wang, X.; Gupta, P.; Mebus, C.A. Efficacy and safety of CE-224,535, an antagonist of P2X₇ receptor, in treatment of patients with rheumatoid arthritis inadequately controlled by methotrexate. *J. Rheumatol.*, **2012**, 39 (4), 720-727.
- [101] Guile, S.D.; Ebden, M. Quinoline derivatives for the treatment of inflammatory diseases. PCT Appl. N. WO 2008114002, September 25, 2008.
- [102] Guile, S.D.; Thompson, T. A quinoline derivative acting as a P2X₇-receptor antagonist. PCT Appl. N. WO 2009070116, June 4, 2009.
- [103] Xiao, Y.; Karra, S.; Goutopoulos, A.; Morse, N.T.; Zhang, S.; Dhanabal, M.; Tian, H.; Seenisamy, J.; Jayadevan, J.; Caldwell, R.; Potnick, J.; Bleich, M.; Chekler, E.; Sherer, B.; Sriraman, V. Synthesis and SAR development of quinoline analogs as novel P2X₇ receptor antagonists. *Bioorg. Med. Chem. Lett.*, **2019**, 29 (13), 1660-1664.
- [104] Letavic, M.A.; Lord, B.; Bischoff, F.; Hawryluk, N.A.; Pieters, S.; Rech, J.C.; Sales, Z.; Velter, A.I.; Ao, H.; Bonaventure, P.; Contreras, V.; Jiang, X.; Morton, K.L.; Scott, B.; Wang, Q.;

- Wickenden, A.D.; Carruthers, N.I.; Bhattacharya, A. Synthesis and pharmacological characterization of two novel, brain penetrating P2X7 antagonists. *ACS Med. Chem. Lett.*, **2013**, *4* (4), 419-422.
- [105] Kilburn, J.P.; Rasmussen, L.K.; Jessing, M.; Eldemenky, E.M.; Chen, B.; Jiang, Y.; Hopper, A.T. Benzamides. PCT Appl. N. WO 2014057078, April 17, 2014.
- [106] Kilburn, J.P.; Rasmussen, L.K.; Jessing, M.; Eldemenky, E.M.; Chen, B.; Jiang, Y. N-(2-(cyclic amine)ethyl)benzamide derivatives as P2X7 inhibitors. PCT Appl. N. WO 2014057080, April 17, 2014.
- [107] Kilburn, J.P.; Hopper, A.T.; Juhl, M. Inhibitor of the P2X7 receptor. PCT Appl. N. WO 2017076825, May 11, 2014.
- [108] Hopper, A.T.; Juhl, M.; Hornberg, J.; Badolo, L.; Kilburn, J.P.; Thougard, A.; Smagin, G.; Song, D.; Calice, L.; Menon, V.; Dale, E.; Zhang, H.; Cajina, M.; Nattini, M.E.; Gandhi, A.; Grenon, M.; Jones, K.; Khayrullina, T.; Chandrasena, G.; Thomsen, C.; Zorn, S.H.; Brodbeck, R.; Poda, S.B.; Staal, R.; Möller, T. Synthesis and Characterization of the Novel Rodent-Active and CNS-Penetrant P2X7 Receptor Antagonist Lu AF27139. *J. Med. Chem.*, **2021**, *64* (8), 4891-4902.
- [109] Love, C.J.; Leenaerts, J.E.; Coymans, L.P.; Lebsack, A.D.; Branstetter, B.J.; Rech, J.C.; Gleason, E.A.; Venable, J.D.; Wiener, D.; Smith, D.M.; Breitenbucher, J.G. PCT Appl. N. WO 2009132000, October 29, 2009.
- [110] Rech, J.C.; Bhattacharya, A.; Branstetter, B.J.; Love, C.J.; Leenaerts, J.E.; Coymans, L.P.; Eckert, W.A.; Ao, H.; Wang, Q.; Chaplan, S.R.; Wickenden, A.D.; Lebsack, A.D.; Breitenbucher, J.G. The discovery and preclinical characterization of 6-chloro-N-(2-(4,4-difluoropiperidin-1-yl)-2-(2-(trifluoromethyl)pyrimidin-5-yl)ethyl)quinoline-5-carboxamide based P2X7 antagonists. *Bioorg. Med. Chem. Lett.*, **2016**, *26* (19), 4781-4784.
- [111] Dean, D.K.; Munoz-Muriedas, J.; Sime, M.; Steadman, J.G.A.; Thewlis, R.E.A.; Trani, G.; Walter, D.S. 5,6,7,8-Tetrahydro[1,2,4]triazolo[4,3-a]pyrazine derivatives as P2X7 modulators. PCT Appl. N. WO 2010125102, November 4, 2010.

- [112] Rudolph, D.A.; Alcazar, J.; Ameriks, M.K.; Anton, A.B.; Ao, H.; Bonaventure, P.; Carruthers, N.I.; Chrovian, C.C.; De Angelis, M.; Lord, B.; Rech, J.C.; Wang, Q.; Bhattacharya, A.; Andres, J.I.; Letavic, M.A. Novel methyl substituted 1-(5,6-dihydro-[1,2,4]triazolo[4,3-a]pyrazin-7(8H)-yl)methanones are P2X7 antagonists. *Bioorg. Med. Chem. Lett.*, **2015**, *25* (16), 3157-3163.
- [113] Chrovian, C.C.; Soyode-Johnson A.; Ao, H.; Bacani, G.M.; Carruthers, N.I.; Lord, B.; Nguyen, L.; Rech, J.C.; Wang, Q.; Bhattacharya, A.; Letavic, M.A. Novel phenyl-substituted 5,6-dihydro-[1,2,4]triazolo[4,3-a]pyrazine P2X7 antagonists with robust target engagement in rat brain. *ACS Chem. Neurosci.*, **2016**, *7* (4), 490-497.
- [114] Savall, B.M.; Wu, D.; De Angelis, M.; Carruthers, N.I.; Ao, H.; Wang, Q.; Lord, B.; Bhattacharya, A.; Letavic, M.A. Synthesis, SAR, and pharmacological characterization of brain penetrant P2X7 receptor antagonists. *ACS Med. Chem. Lett.*, **2015**, *6* (6), 671-676.
- [115] Letavic, M.A.; Savall, B.M.; Allison, B.D.; Aluisio, L.; Andres, J.I.; De Angelis, M.; Ao, H.; Beauchamp, D.A.; Bonaventure, P.; Bryant, S.; Carruthers, N.I.; Ceusters, M.; Coe, K. J.; Dvorak, C.A.; Fraser, I.C.; Gelin, C.F.; Koudriakova, T.; Liang, J.; Lord, B.; Lovenberg, T.W.; Otieno, M.A.; Schoetens, F.; Swanson, D.M.; Wang, Q.; Wickenden, A.D.; Bhattacharya, A. 4-Methyl-6,7-dihydro-4H-triazolo[4,5-c]pyridine-Based P2X7 Receptor Antagonists: Optimization of Pharmacokinetic Properties Leading to the Identification of a Clinical Candidate. *J. Med. Chem.*, **2017**, *60* (11), 4559-4572.
- [116] Swanson, D.M.; Savall, B.M.; Coe, K.J.; Schoetens, F.; Koudriakova, T.; Skaptason, J.; Wall, J.; Rech, J.; Deng, X.; De Angelis, M.; Everson, A.; Lord, B.; Wang, Q.; Ao, H.; Scott, B.; Sepassi, K.; Lovenberg, T.W.; Carruthers, N.I.; Bhattacharya, A.; Letavic, M.A. Identification of (R)-(2-Chloro-3-(trifluoromethyl)phenyl)(1-(5-fluoropyridin-2-yl)-4-methyl-6,7-dihydro-1H-imidazo[4,5-c]pyridin-5(4H)-yl)methanone (JNJ 54166060), a small molecule antagonist of the P2X7 receptor. *J. Med. Chem.*, **2016**, *59* (18), 8535-8548.
- [117] Ziff, J.; Rudolph, D.A.; Stenne, B.; Koudriakova, T.; Lord, B.; Bonaventure, P.; Lovenberg, T.W.; Carruthers, N.I.; Bhattacharya, A.; Letavic, M.A.; Shireman, B.T. Substituted 5,6-

(Dihydropyrido[3,4-*d*]pyrimidin-7(8*H*)-yl)-methanones as P2X7 antagonists. *ACS Chem. Neurosci.*, **2016**, 7 (4), 498-504.

[118] Ameriks, M.K.; Ao, H.; Carruthers, N.I.; Lord, B.; Ravula, S.; Rech, J.C.; Savall, B.M.; Wall, J.L.; Wang, Q.; Bhattacharya, A.; Letavic, M.A. Preclinical characterization of substituted 6,7-dihydro-[1,2,4]triazolo[4,3-*a*]pyrazin-8(5*H*)-one P2X7 receptor antagonists. *Bioorg. Med. Chem. Lett.*, **2016**, 26 (2), 257-261.

[119] Carroll, W.A.; Perez-Medrano, A.; Florjancic, A.S.; Nelson, D.W.; Peddi, S.; Li, T.; Bunnelle, E.M.; Hirst, G.C.; Li, B. Amino-tetrazoles analogues and methods of use. PCT Appl. N. WO 2005111003, November 24, 2005.

[120] Carroll, W.A.; A.; Florjancic, A.S.; Perez-Medrano, A.; Peddi, S. P2X7 receptor antagonists and methods of use. PCT Appl. N. WO2007056046, May 18, 2007.

[121] Lopez-Tapia, F.; Walker, K.A.; Brotherton-Pleiss, C.; Caroon, J.; Nitzan, D.; Lowrie, L.; Gleason, S.; Zhao, S.H.; Berger, J.; Cockayne, D.; Phippard, D.; Suttman, R.; Fitch, W.L.; Bourdet, D.; Rege, P.; Huang, X.; Broadbent, S.; Dvorak, C.; Zhu, J.; Wagner, P.; Padilla, F.; Loe, B.; Jahangir, A.; Alker, A. Novel series of dihydropyridinone P2X7 receptor antagonists. *J. Med. Chem.*, **2015**, 58 (21), 8413-8426.

[122] Beswick, P.J.; Chambers, L.J.; Davies, D.J.; Dean, D.K.; Demont, E.H.; Susan Roomans, S.; Walter, D.S. N-(phenylmethyl)-2-(1*H*-pyrazol-4-yl) acetamide derivatives as P2X7 antagonists for the treatment of pain, inflammation and neurodegeneration. PCT Appl. N. WO 2007141267, December 13, 2007.

[123] Beswick, P.J.; Dean, D.K.; Walter, D.S. Pyrazole derivatives as P2X7 modulators. PCT Appl. N. PCT Appl. N. WO 2008125600, October 23, 2008.

[124] Chambers, L.J.; Stevens, A.J.; Moses, A.P.; Michel, A.D.; Walter, D.S.; Davies, D.J.; Livermore, D.G.; Fonfria, E.; Demont, E.H.; Vimal, M.; Theobald, P.J.; Beswick, P.J.; Gleave, R.J.; Roman, S.A.; Senger, S. Synthesis and structure-activity relationships of a series of (1*H*-pyrazol-4-

yl)acetamide antagonists of the P2X7 receptor. *Bioorg. Med. Chem. Lett.*, **2010**, *20* (10), 3161-3164.

[125] Beswick, P.J.; Billinton, A.; Chambers, L.J.; Dean, D.K.; Fonfria, E.; Gleave, R.J.; Medhurst, S.J.; Michel, A.D.; Moses, A.P.; Patel, S.; Roman, S.A.; Roomans, S.; Senger, S.; Stevens, A.J.; Walter, D.S. Structure-activity relationships and in vivo activity of (1*H*-pyrazol-4-yl)acetamide antagonists of the P2X(7) receptor. *Bioorg. Med. Chem. Lett.*, **2010**, *20* (15), 4653-4656.

[126] Gleave, R.J.; Walter, D.S.; Beswick, P.J.; Fonfria, E.; Michel, A.D.; Roman, S.A.; Tang, S.P. Synthesis and biological activity of a series of tetrasubstituted-imidazoles as P2X(7) antagonists. *Bioorg. Med. Chem. Lett.*, **2010**, *20* (16), 4951-4954.

[127] Abdi, M.H.; Beswick, P.J.; Billinton, A.; Chambers, L.J.; Charlton, A.; Collins, S.D.; Collis, K.L.; Dean, D.K.; Fonfria, E.; Gleave, R.J.; Lejeune, C.L.; Livermore, D.G.; Medhurst, S.J.; Michel, A.D.; Moses, A.P.; Page, L.; Patel, S.; Roman, S.A.; Senger, S.; Slingsby, B.; Steadman, J.G.; Stevens, A.J.; Walter, D.S. Discovery and structure-activity relationships of a series of pyroglutamic acid amide antagonists of the P2X7 receptor. *Bioorg. Med. Chem. Lett.*, **2010**, *20* (17), 5080-5084.

[128] Ali, Z.; Laurijssens, B.; Ostefeld, T.; McHugh, S.; Stylianou, A.; Scott-Stevens, P.; Hosking, L.; Dewit, O.; Richardson, J.C.; Chen, C. Pharmacokinetic and pharmacodynamic profiling of a P2X7 receptor allosteric modulator GSK1482160 in healthy human subjects. *Br. J. Clin. Pharmacol.*, **2013**, *75* (1), 197-207.

[129] Abberley, L.; Bebius, A.; Beswick, P.J.; Billinton, A.; Collis, K.L.; Dean, D.K.; Fonfria, E.; Gleave, R.J.; Medhurst, S.J.; Michel, A.D.; Moses, A.P.; Patel, S.; Roman, S.A.; Scoccitti, T.; Smith, B.; Steadman, J.G.; Walter, D.S. Identification of 2-oxo-N-(phenylmethyl)-4-imidazolidinecarboxamide antagonists of the P2X(7) receptor. *Bioorg. Med. Chem. Lett.*, **2010**, *20* (22), 6370-6374.

[130] Wilson, A.W.; Medhurst, S.J.; Dixon, C.I.; Bontoft, N.C.; Winyard, L.A.; Brackenborough, K.T.; De Alba, J.; Clarke, C.J.; Gunthorpe, M.J.; Hicks, G.A.; Bountra, C.; McQueen, D.S.;

- Chessell, I.P. An animal model of chronic inflammatory pain: pharmacological and temporal differentiation from acute models. *Eur. J. Pain.*, **2006**, *10* (6), 537-549.
- [131] Betschmann, P.; Carroll, W.A.; Ericsson, A.M.; Fix-Stenzel, S.R.; Friedman, M.; Hirst, G.C.; Josephsohn, N.S.; Li, B.; Perez-Medrano, A.; Morytko, M.J.; Rafferty, P.; Chen, H. Piperazines as P2X7 antagonists. PCT Appl. N. WO 2008005368, January 10, 2008.
- [132] Morytko, M.J.; Betschmann, P.; Woller, K.; Ericsson, A.; Chen, H.; Donnelly-Roberts, D.L.; Namovic, M.T.; Jarvis, M.F.; Carroll, W.A.; Rafferty, P. Synthesis and in vitro activity of N'-cyano-4-(2-phenylacetyl)-N-o-tolylpiperazine-1-carboximidamide P2X7 antagonists. *Bioorg. Med. Chem. Lett.*, **2008**, *18* (6), 2093-2096.
- [133] Patberg, M.; Isaak, A.; Füsser, F.; Ortiz Zacarías, N.V.; Vinnenberg, L.; Schulte, J.; Michetti, L.; Grey, L.; van der Horst, C.; Hundehege, P.; Koch, O.; Heitman, L.H.; Budde, T.; Junker, A. Piperazine squaric acid diamides, a novel class of allosteric P2X7 receptor antagonists. *Eur. J. Med. Chem.*, **2021**, *226*, 113838.
- [134] O'Brien-Brown, J. Jackson, A. Reekie, T.A.; Barron, M.L.; Werry, E.L.; Schiavini, P.; McDonnell, M.; Munoz, L.; Wilkinson, S.; Noll, B.; Wang, S.; Kassiou, M. Discovery and pharmacological evaluation of a novel series of adamantyl cyanoguanidines as P2X7 receptor antagonists. *Eur. J. Med. Chem.*, **2017**, *130*, 433-439.
- [135] Calzaferri, F.; Narros-Fernández, P.; de Pascual, R.; de Diego, A.M.G.; Nicke, A.; Egea, J.; García, A.G.; de Los Ríos, C. Synthesis and pharmacological evaluation of novel non-nucleotide purine derivatives as P2X7 antagonists for the treatment of neuroinflammation. *J. Med. Chem.*, **2021**, *64* (4), 2272-2290.
- [136] Faria, R.X.; Oliveira, F.H.; Salles, J.P.; Oliveira, A.S.; von Ranke, N.L.; Bello, M.L.; Rodrigues, C.R.; Castro, H.C.; Louvis, A.R.; Martins, D.L.; Ferreira, V.F. 1,4-Naphthoquinones potently inhibiting P2X7 receptor activity. *Eur. J. Med. Chem.*, **2018**, *143*, 1361-1372.
- [137] Pacheco, P.A.F.; Galvão, R.M.S.; Faria, A.F.M.; Von Ranke, N.L., Rangel, M.S.; Ribeiro, T.M.; Bello, M.L. Rodrigues, C.R., Ferreira, V.F.; da Rocha, D.R., Faria, R.X. 8-Hydroxy-2-(1H-

1,2,3-triazol-1-yl)-1,4-naphthoquinone derivatives inhibited P2X7 Receptor-Induced dye uptake into murine Macrophages. *Bioorg. Med. Chem.*, **2019**, *27* (8), 1449-1455.

[138] Pisylyagin, E.; Kozlovskiy, S.; Menchinskaya, E.; Chingizova, E.; Likhatskaya, G.; Gorpenchenko, T.; Sabutski, Y.; Polonik, S.; Aminin, D. Synthetic 1,4-naphthoquinones inhibit P2X7 receptors in murine neuroblastoma cells. *Bioorg. Med. Chem.*, **2021**, *31*, 115975.

[139] Park, J.H.; Lee, G.E.; Lee, S.D.; Hien, T.T.; Kim, S.; Yang, J.W.; Cho, J.H.; Ko, H.; Lim, S.C.; Kim, Y.G.; Kang, K.W.; Kim, Y.C. Discovery of novel 2,5-dioxoimidazolidine-based P2X(7) receptor antagonists as constrained analogues of KN62. *J. Med. Chem.*, **2015**, *58* (5), 2114-2134.

[140] Park, J.H.; Lee, G.E.; Lee, S.D.; Ko, H.; Kim, Y.C. Structure-activity relationship studies of pyrimidine-2,4-dione derivatives as potent P2X7 receptor antagonists. *Eur. J. Med. Chem.*, **2015**, *106*, 180-193.

[141] Matasi, J.J.; Brumfield, S.; Tulshian, D.; Czarnecki, M.; Greenlee, W.; Garlisi, C.G.; Qiu, H.; Devito, K.; Chen, S.C.; Sun, Y.; Bertorelli, R.; Geiss, W.; Le, V.D.; Martin, G.S.; Vellekoop, S.A.; Haber, J.; Allard, M.L. Synthesis and SAR development of novel P2X7 receptor antagonists for the treatment of pain: part 1. *Bioorg. Med. Chem. Lett.*, **2011**, *21* (12), 3805-3808.

[142] Mahmood, A.; Ali Shah, S.J.; Iqbal, J. Design and synthesis of adamantane-1-carbonyl thiourea derivatives as potent and selective inhibitors of h-P2X4 and h-P2X7 receptors: An Emerging therapeutic tool for treatment of inflammation and neurological disorders. *Eur. J. Med. Chem.*, **2022**, *231*, 114162.

[143] Rudin, M.; Weissleder, R. Molecular imaging in drug discovery and development. *Nat. Rev. Drug Discov.*, **2003**, *2* (2), 123-131.

[144] Pike, V.W. Considerations in the development of reversibly binding PET radioligands for brain imaging. *Curr. Med. Chem.*, **2016**, *23* (18), 1818–1869.

[145] Janssen, B.; Vugts, D.J.; Windhorst, A.D.; Mach, R.H. PET imaging of microglial activation beyond targeting TSPO. *Molecules*, **2018**, *23* (3), 607.

- [146] Janssen, B.; Ory, D.; Wilkinson, S.M.; Vugts, D.J.; Kooijman, E.; Verbeek, J.; Funke, U.; Molenaar, G.T.; Kruijer, P.S.; Lammertsma, A.A.; Kassiou, M.; Bormans, G.; Windhorst, A.D. Initial evaluation of P2X7R antagonists [11C]A-740003 and [11C]SMW64-D16 as PET tracers of microglial activation in neuroinflammation. *J. Labelled Comp. Radiopharm.*, **2015**, *58* (S1), S277.
- [147] Janssen, B.; Vugts, D.J.; Wilkinson, S.M.; Ory, D.; Chalon, S.; Hoozemans, J.J.M.; Schuit, R.C.; Beaino, W.; Kooijman, E.J.M.; van den Hoek, J.; Chishty, M.; Doméné, A.; Van der Perren, A.; Villa, A.; Maggi, A.; Molenaar, G.T.; Funke, U.; Shevchenko, R.V.; Baekelandt, V.; Bormans, G.; Lammertsma, A.A.; Kassiou, M.; Windhorst, A.D. Identification of the allosteric P2X7 receptor antagonist [11C]SMW139 as a PET tracer of microglial activation. *Sci. Rep.*, **2018**, *8* (1), 6580.
- [148] Hagens, M.H.J.; Golla, S.S.V.; Janssen, B.; Vugts, D.J.; Beaino, W.; Windhorst, A.D.; O'Brien-Brown, J.; Kassiou, M.; Schuit, R.C.; Schwarte, L.A.; de Vries, H.E.; Killestein, J.; Barkhof, F.; van Berckel, B.N.M.; Lammertsma, A.A. The P2X7 receptor tracer [11C]SMW139 as an in vivo marker of neuroinflammation in multiple sclerosis: a first-in man study. *Eur. J. Nucl. Med. Mol. Imaging*, **2020**, *47* (2), 379-389.
- [149] Territo, P.R.; Meyer, J.A.; Peters, J.S.; Riley, A.A.; McCarthy, B.P.; Gao, M.; Wang, M.; Green, M.A.; Zheng, Q.H.; Hutchins, G.D. Characterization of 11C-GSK1482160 for targeting the P2X7 receptor as a biomarker for neuroinflammation. *J. Nucl. Med.*, **2017**, *58* (3), 458-465.
- [150] Han, J.; Liu, H.; Liu, C.; Jin, H.; Perlmutter, J.S.; Egan, T.M.; Tu, Z. Pharmacologic characterizations of a P2X7 receptor-specific radioligand, [11C]GSK1482160 for neuroinflammatory response. *Nucl. Med. Commun.*, **2017**, *38* (5), 372-382.
- [151] Green, M.; Hutchins, G.; Fletcher, J.; Territo, W.; Polson, H.; Trussel, H.; Wissman, C.; Zheng, Q-H.; Gao, M.; Wang, M.; Glick-Wilson, B. Distribution of the P2X7-receptor-targeted [11C]GSK1482160 radiopharmaceutical in normal human subjects. *J. Nucl. Med.*, **2018**, *59* (supplement 1), 1009.

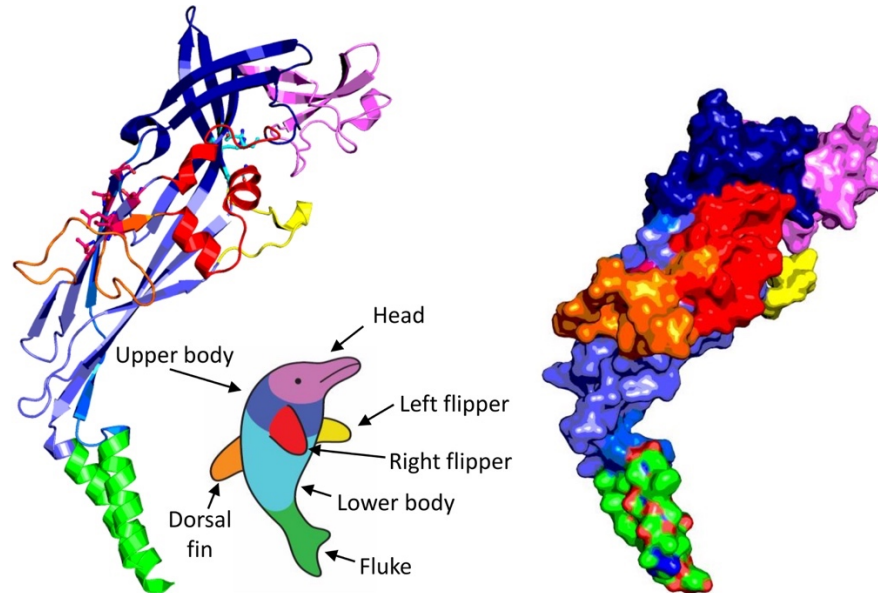
- [152] Gao, M.; Wang, M.; Meyer, J.A.; Territo, P.R.; Hutchins, G.D.; Zarrinmayeh, H.; Zheng, Q.H. Synthesis and in vitro biological evaluation of new P2X7R radioligands [11C]halo-GSK1482160 analogs. *Bioorg. Med. Chem. Lett.*, **2019**, *29* (12), 1476-1480.
- [153] Ory, D.; Celen, S.; Gijsbers, R.; Van Den Haute, C.; Postnov, A.; Koole, M.; Vandeputte, C.; Andrés, J.I.; Alcazar, J.; De Angelis, M.; Langlois, X.; Bhattacharya, A.; Schmidt, M.; Letavic, M.A.; Vanduffel, W.; Van Laere, K.; Verbruggen, A.; Debyser, Z.; Bormans, G. Preclinical evaluation of a P2X7 receptor-selective radiotracer: PET studies in a rat model with local overexpression of the human P2X7 receptor and in nonhuman primates. *J. Nucl. Med.*, **2016**, *57* (9), 1436-1441.
- [154] Van Weehaeghe, D.; Koole, M.; Schmidt, M.E.; Deman, S.; Jacobs, A.H.; Souche, E.; Serdons, K.; Sunaert, S.; Bormans, G.; Vandenberghe, W.; Van Laere, K. [11C]JNJ54173717, a novel P2X7 receptor radioligand as marker for neuroinflammation: human biodistribution, dosimetry, brain kinetic modelling and quantification of brain P2X7 receptors in patients with Parkinson's disease and healthy volunteers. *Eur. J. Nucl. Med. Mol. Imaging*, **2019**, *46* (10), 2051-2064.
- [155] Fantoni, E.R.; Dal Ben, D.; Falzoni, S.; Di Virgilio, F.; Lovestone, S.; Gee, A. Design, synthesis and evaluation in an LPS rodent model of neuroinflammation of a novel 18F-labelled PET tracer targeting P2X7. *E.J.N.M.M.I. Res.*, **2017**, *7* (1), 31.
- [156] Koole, M.; Schmidt, M.E.; Hijzen, A.; Ravenstijn, P.; Vandermeulen, C.; Van Weehaeghe, D.; Serdons, K.; Celen, S.; Bormans, G.; Ceusters, M.; Zhang, W.; Van Nueten, L.; Kolb, H.; de Hoon, J.; Van Laere, K. 18F-JNJ-64413739, a novel PET ligand for the P2X7 ion channel: radiation dosimetry, kinetic modeling, test-retest variability, and occupancy of the P2X7 antagonist JNJ-54175446. *J. Nucl. Med.*, **2019**, *60* (5), 683-690.
- [157] Mertens, N.; Schmidt, M.E.; Hijzen, A.; Van, Weehaeghe, D.; Ravenstijn, P.; Depre, M.; de Hoon, J.; Van Laere, K.; Koole, M. Minimally invasive quantification of cerebral P2X7R

occupancy using dynamic [18F]JNJ-64413739 PET and MRA-driven image derived input function. *Sci. Rep.*, **2021**, *11* (1), 16172.

[158] Morgan, J.; Moreno, O.; Alves, M.; Baz, Z.; Menéndez Méndez, A.; Leister, H.; Melia, C.; Smith, J.; Visekruna, A.; Nicke, A.; Bhattacharya, A.; Ceusters, M.; Henshall, D.C.; Gómez-Vallejo, V.; Llop, J.; Engel, T. Increased uptake of the P2X7 receptor radiotracer 18 F-JNJ-64413739 in the brain and peripheral organs according to the severity of status epilepticus in male mice. *Epilepsia*, **2023**, *64* (2), 511-523.

[158] Fu, Z.; Lin, Q.; Hu, B.; Zhang, Y.; Chen, W.; Zhu, J.; Zhao, Y.; Choi, H.S.; Shi, H.; Cheng, D. P2X7 PET radioligand 18F-PTTP for differentiation of lung tumor from inflammation. *J. Nucl. Med.*, **2019**, *60* (7), 930-936.

Fig. (1). Dolphin-like shape of the single subunit of the P2X7 receptor, sequence coloring refers to the respective dolphin parts. Pink and cyan rectangles indicate the ATP-binding site formed at the interface of two different subunits.



TMPACCSWKDVFQYETNKVLRIQSTNYG**TIKWIFHVLVFSYISFALISDKRYQKKEPLISSVHTKVK**GIAEVKAEILENG
 MKKMVSGVFDADYTFPLQGNSEFFVMTNFIKTEGQQQLCPDFPTRRTICSSDRGCKKGRMDPQSKGIQTGRCV
 VYKERLKTCEVSAWCPIEEVEDA**PRPALLNSAENFTVLIKNNIDFPGHNYTTRNILPGVNITCTFHKTQNPQCFIRLG**
DIFQETGDNFSDVAIQGGIMGIEIYWDCNLDGWFHHCPRPKYSFRR**LDDKTTNESLYPGYNFRYAKYYKENVKERT**
LIKVFGIRFDILVFGTGGKFVNIQLAVYIGSVISYFGLATVFIDIINTYSSKCCRSRIYPCFKCCEYCAVNEYYYRKQSEPI
 AEPKPTLKYVSFVDETHIRMVDQQLGKSLQNVKGEKVQRPSVDFTDL SRLSLSLCDPTPIPGQPEEMQLFSEEVTPR
 SSNSPDWCQCGHCLPSQLPESHRCLEELCCRKKAGACITTSEPFKRLVLSRQVLQFLLLYQEPLLVLDGNSSSRLRHCA
 YRCYTTWRFGSPDLADFAILPSCCRWRIRREFPKSEGQYTGFSQSPY

Fig. (2). The general architecture of P2X7 homotrimer, a) apo form: 5U1L, b) & c) ATP (cyan)- and ligand (magenta)-bound form: 5U2H crystal, d) ligand-protein interaction matrix for different giant panda crystals (for simplicity, each crystal is depicted in different color).

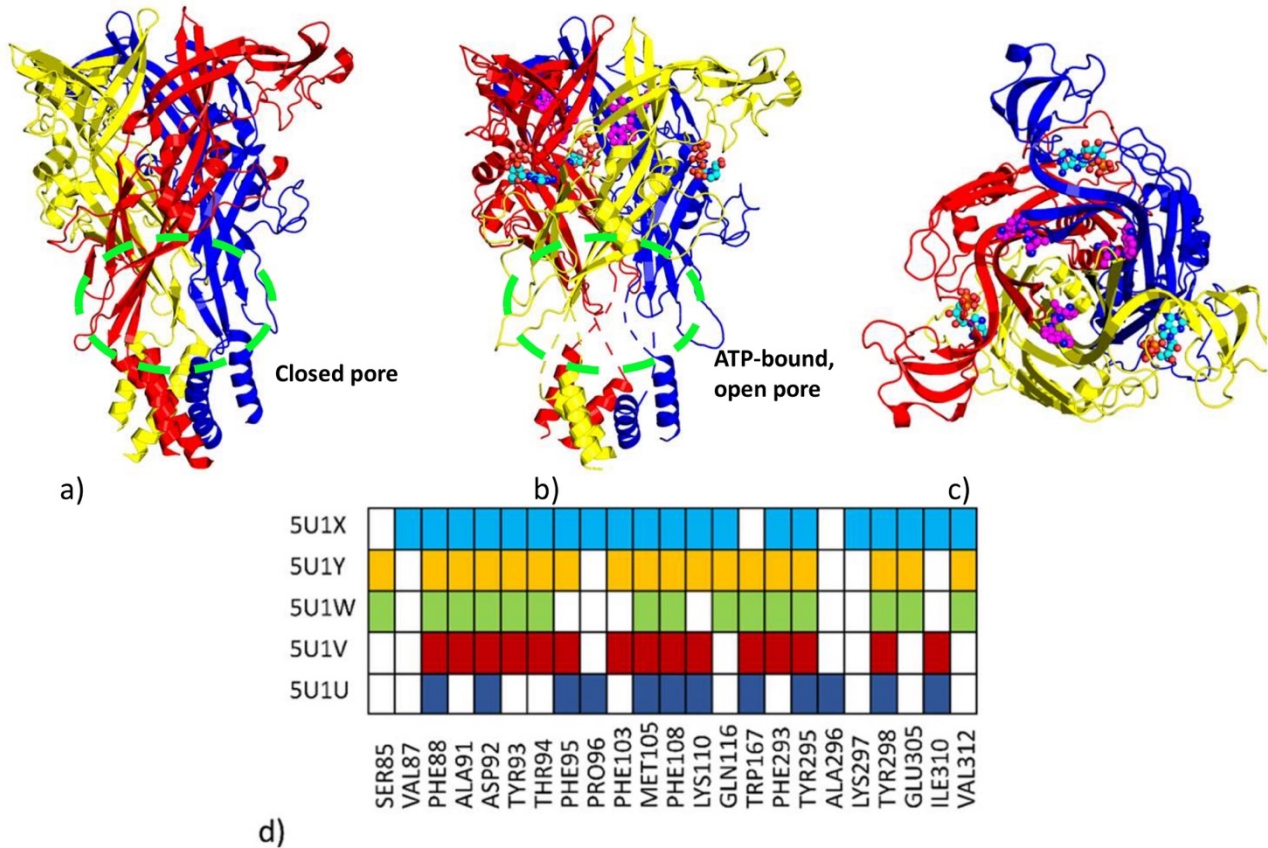


Fig. (3). Downstream pathway triggered by P2X7R activation leading to inflammasome NLRP3 activation and consequent IL-1 β and IL-18 release.

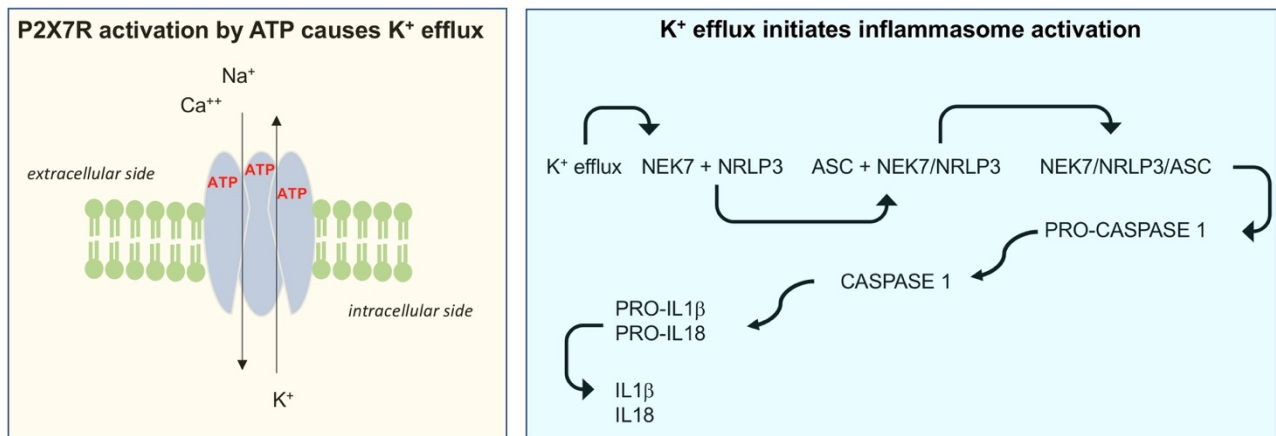
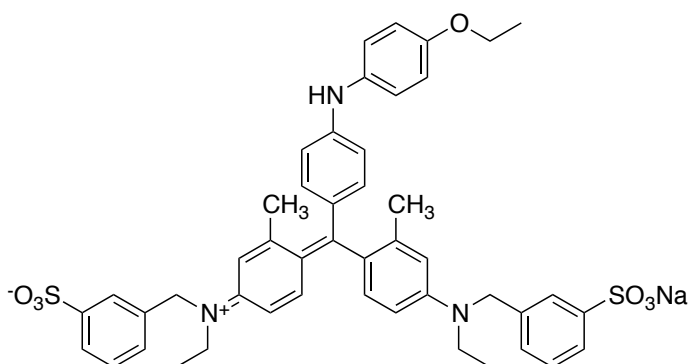
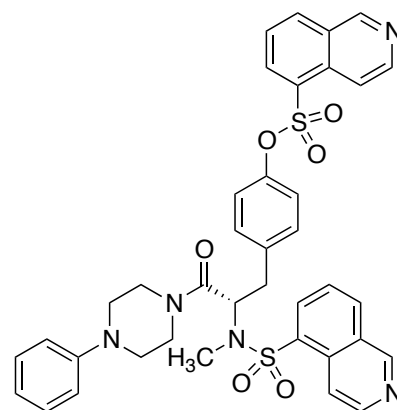


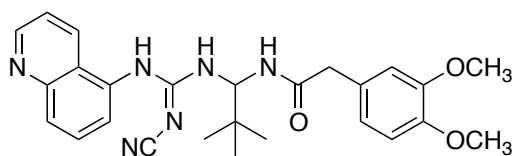
Fig. (4). First and second generation of P2X7R antagonists (data taken from references 84-88).



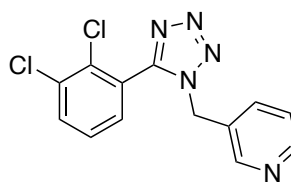
BBG
hP2X7 IC_{50} = 200 nM
rP2X7 IC_{50} = 10 nM



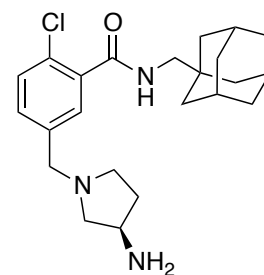
KN-62
hP2X7 IC_{50} = 15 nM
rP2X7 inactive



A-740003
hP2X7 IC_{50} = 44nM
rP2X7 IC_{50} = 18 nM



A-438079
hP2X7 pIC_{50} = 6.5



GSK-314181A
hP2X7 pIC_{50} = 9.0

Fig. (5). Interaction of the co-crystallized ligands with the P2X7R in different crystal structures; coloring in the ligand-protein complexes and in the ligand-protein interaction matrix indicates amino acids which make contacts with the corresponding parts of the ligands; for simplicity, ligands in the presented complexes are depicted in gray and coloring of its respective parts is shown beside.

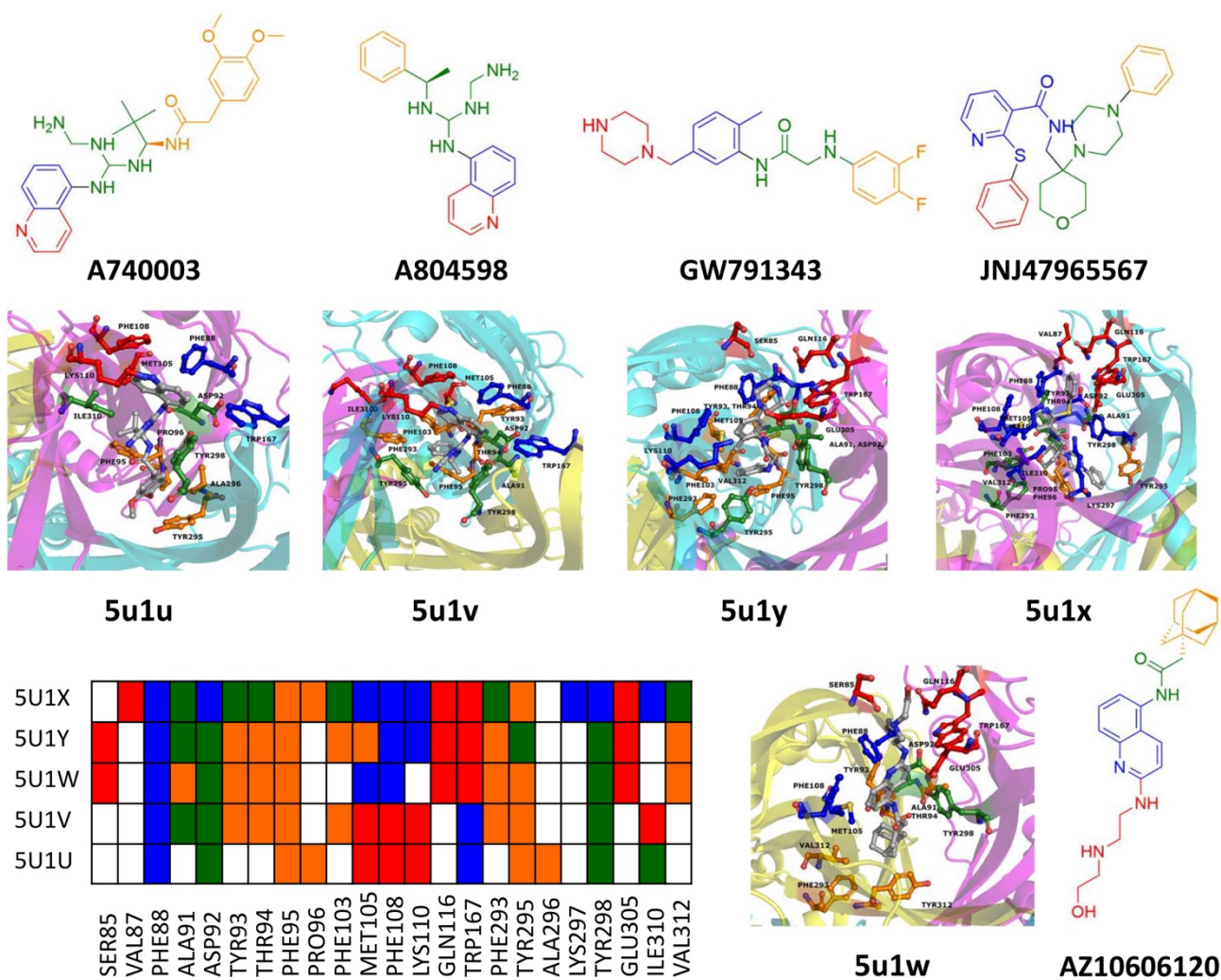


Fig. (6). Structure of a representative adamantane amide described by Astra Zeneca [93]

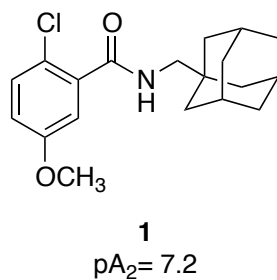
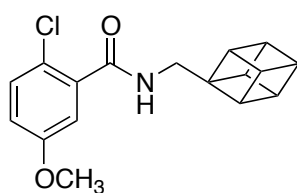
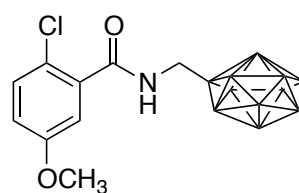


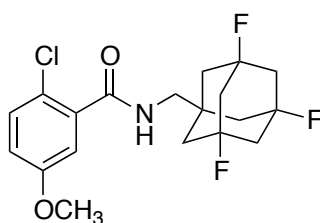
Fig. (7). Chemical structures of polycyclic benzamides **2-4** [94, 95]



2
hP2X7R pIC₅₀ = 7.98^a



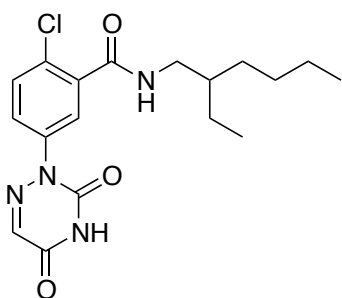
3
hP2X7R pIC₅₀ = 8.07^a



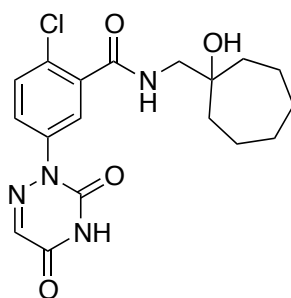
4 (SMW139)
hP2X7R IC₅₀ = 33.9 nM^a
mP2X7R IC₅₀ = 158 nM^b

^aActivity assessed as dye uptake inhibition assay in THP-1 cells. ^bActivity assessed by a Ca²⁺ influx assay in THP-1 cells.

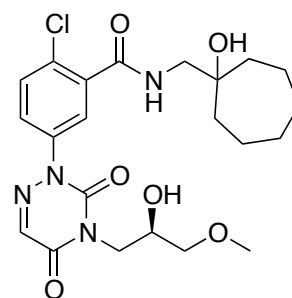
Fig. (8). The activity of 6-azauracil benzamides **8-10**, assessed as hIL-1 β release inhibition derived from monocytes stimulated by ATP [98]



8
hIL-1 β inhibition IC₅₀ = 0.8 μ M
clogP = 4.45

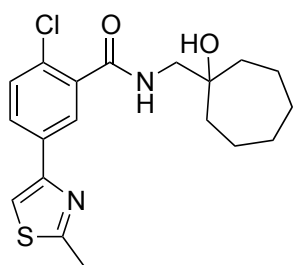


9
hIL-1 β inhibition IC₅₀ = 83 nM
clogP = 2.9

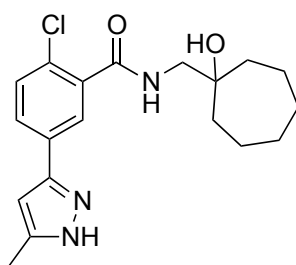


10 (CE-224535)
hIL-1 β inhibition IC₅₀ = 0.001 nM
clogP = 2.6

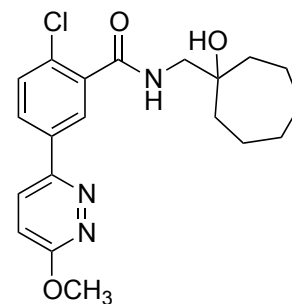
Fig. (9). Azinyl- and azolylbenzamides as hP2X7R antagonists. Activity assessed as YO PRO dye uptake inhibition assay [99]



11
hP2X7R IC₅₀ = 0.006 μM

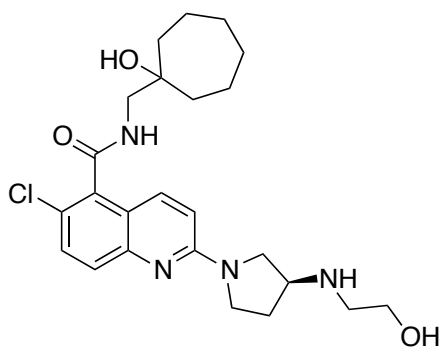


12
hP2X7R IC₅₀ = 0.003 μM

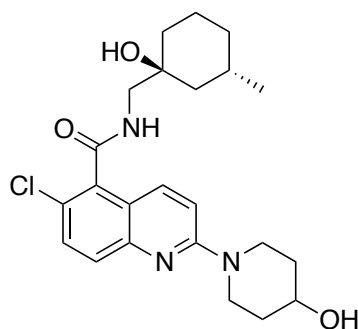


13
hP2X7R IC₅₀ = 0.028 μM

Fig. (10). 6-Chloroquinoline-5-carboxamides patented by AstraZeneca [101, 102]



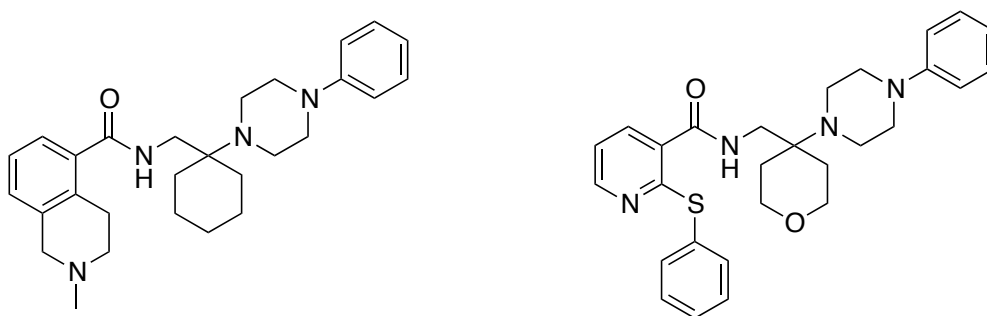
14
hP2X7R pIC₅₀ = 8.4



15
hP2X7R pIC₅₀ = 8.1

Fig. (11). Potent brain penetrant P2X7 antagonists. pIC₅₀ values were measured in a Ca²⁺ flux assay

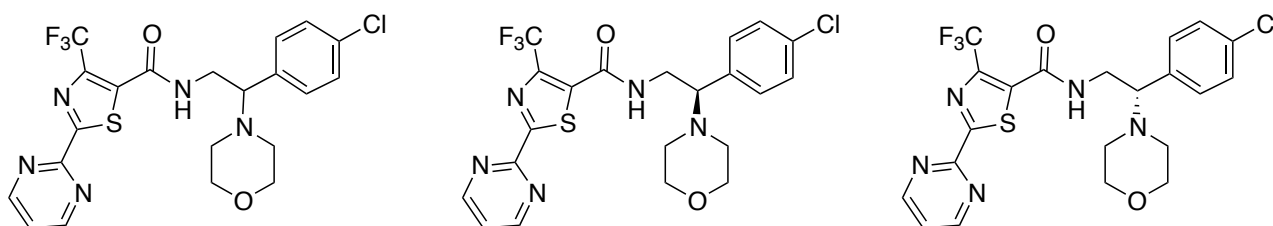
[104]



23 (JNJ-42253432)
hP2X7R pIC₅₀ = 7.7
rP2X7R pIC₅₀ = 7.8

24 (JNJ-42253432)
hP2X7R pIC₅₀ = 8.3
rP2X7R pIC₅₀ = 7.2

Fig. (12). Thiazol-5-carboxamide derivatives [108]

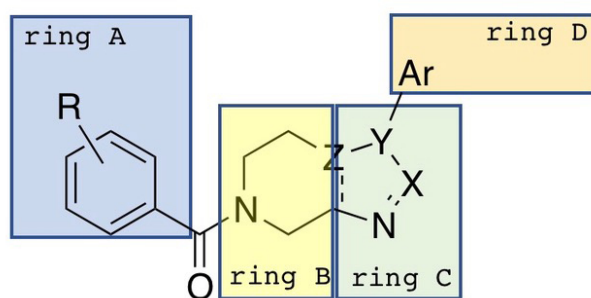


33
hP2X7R IC₅₀ = 32 nM

(S)-33
hP2X7R IC₅₀ = 12 nM

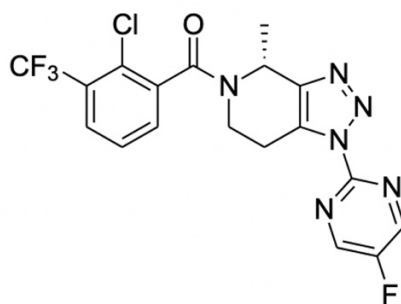
(R)-33
hP2X7R IC₅₀ = 89 nM

Fig. (13). General formula of rigidified benzamides



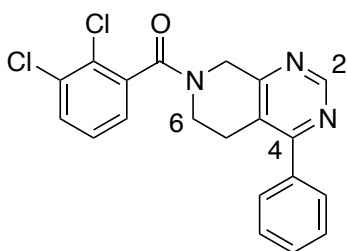
X, Y, Z = CH or N

Fig. (14). Structural formula and activity data of compound JNJ-541754446 [115]

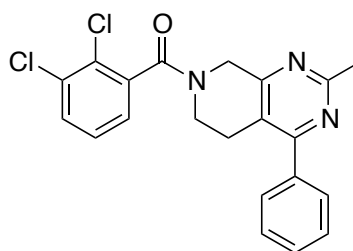


JNJ-54175446
hP2X7R pIC_{50} = 8.46
rP2X7R pIC_{50} = 8.81
Human dose predicted = 8 mg q.d.

Fig. (15). Structural formulas and activity data of compounds **73** and **74** [117]

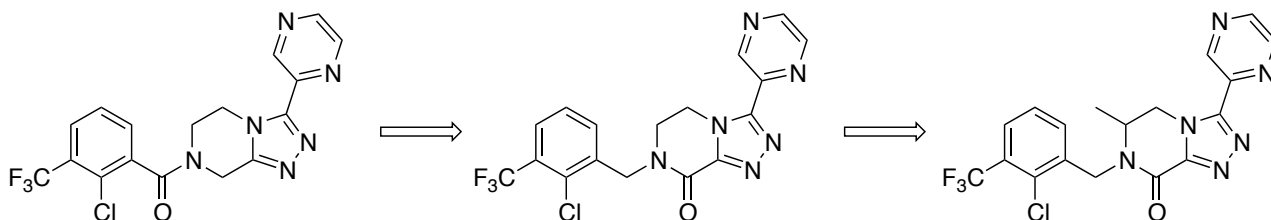


73
hP2X7R IC_{50} = 48 nM
rP2X7R IC_{50} = 4860 nM
metabolic stability (extraction rate) = 0.74
cLogP = 4.1



74
hP2X7R IC_{50} = 120 nM
rP2X7R IC_{50} = 4600 nM
metabolic stability (extraction rate) = 0.3
cLogP = 4.6

Fig. (16). Design of benzyl lactam derivatives **79** and **80** [118]

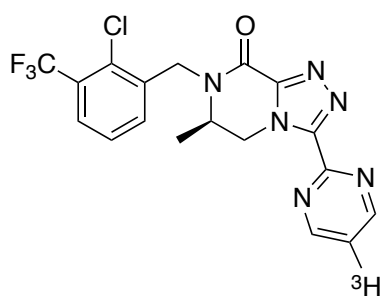


50
hP2X7R IC_{50} = 2.1 nM
rP2X7R IC_{50} = 92 nM

79
hP2X7R IC_{50} = 440 nM
rP2X7R IC_{50} = 8670 nM

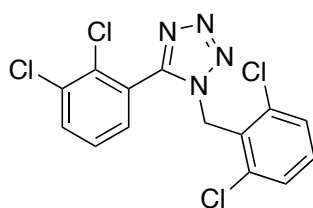
80
hP2X7R IC_{50} = 3.4 nM
rP2X7R IC_{50} = 36 nM

Fig. (17). Structural formula of P2X7R radioligand [³H]JNJ-54232334

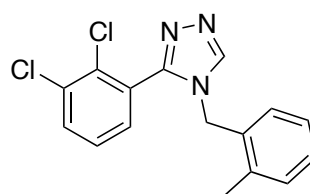


[³H] JNJ-54232334

Fig. (18). Tetrazole and triazole amide isosteres [119, 120]

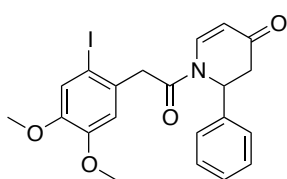


84 (A-438079)
hP2X7R pIC₅₀ = 6.9
rP2X7R pIC₅₀ = 6.5

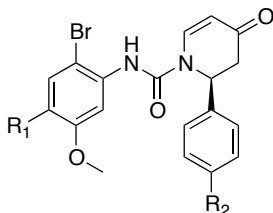


85
hP2X7R pIC₅₀ = 7.1
rP2X7R pIC₅₀ = 6.7

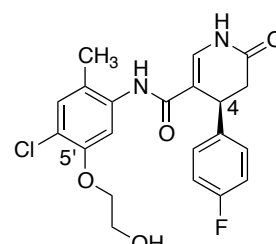
Fig. (19). Activity data of dihydropyridinone P2X7R antagonists. IC₅₀ values were determined using a FLIPR Ca²⁺ flux assay using 1321N1 cells expressing hP2X7R [121]



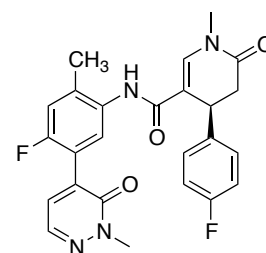
86
hP2X7R IC₅₀ = 104 nM
HLM CL_{int} = 168 μL/min/mg
RLM CL_{int} = 548 μL/min/mg



87 R₁ = Cl; R₂ = H hP2X7R IC₅₀ = 33 nM
88 R₁ = Cl; R₂ = F hP2X7R IC₅₀ = 37 nM
89 R₁ = F; R₂ = F hP2X7R IC₅₀ = 33 nM



90
hP2X7R IC₅₀ = 23 nM
positive to Ames test



91
hP2X7R IC₅₀ = 8 nM
negative to Ames test

Fig. (20). SAR summary of aliphatic amides related to compound **92** [124]

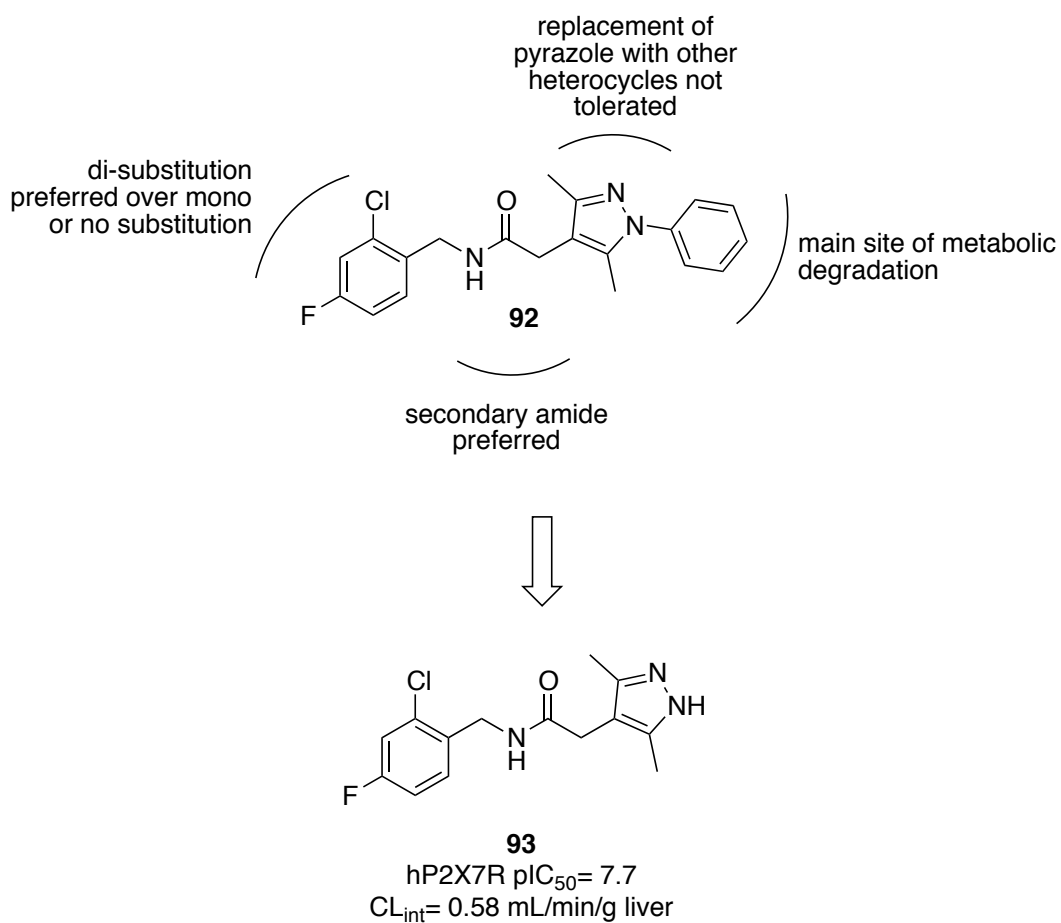


Fig. (21). Structural evolution from pyrazole to imidazole derivatives [124, 126]

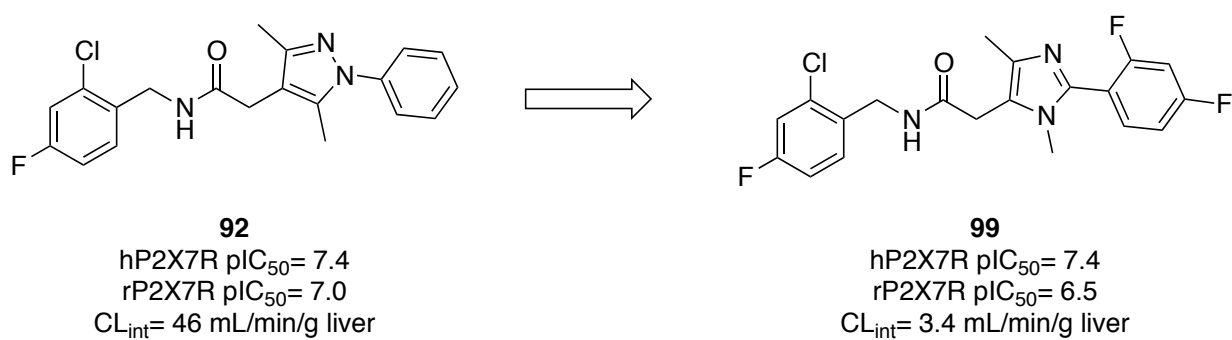


Fig. (22). Development of P2X7R antagonists with pyrrolidinone structure [127]

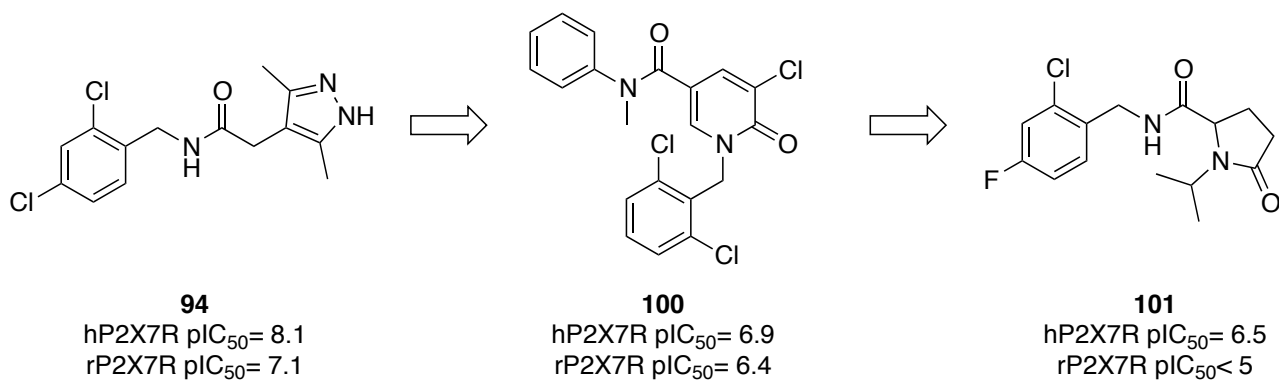


Fig. (23). Structure of the 2-oxoimidazolidine-4-carboxamide derivative **115** [129]

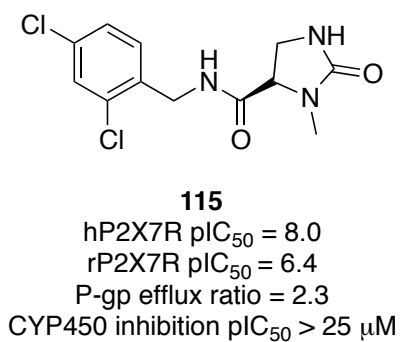
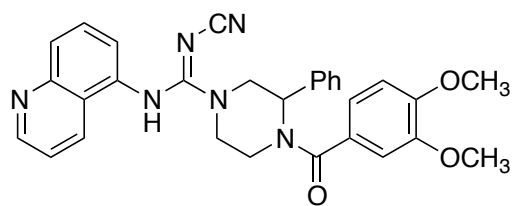
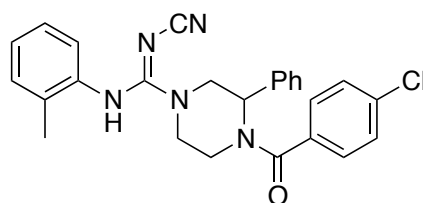


Fig. (24). Squaric acid diamide derivatives. pIC₅₀ generated using the YO-PRO-1 uptake assay

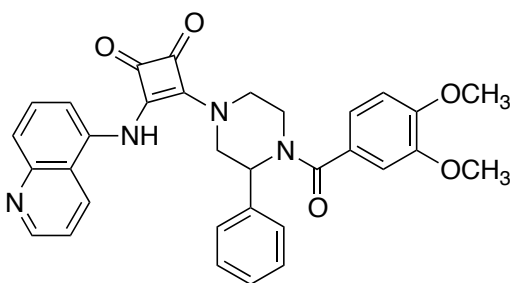
[132-133]



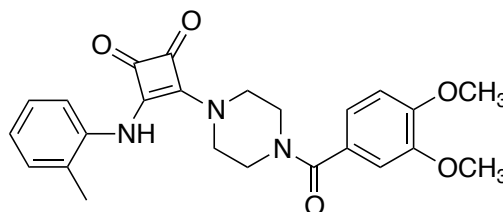
116
hP2X7R pIC₅₀ = 7.2
rP2X7R pIC₅₀ = 7.5



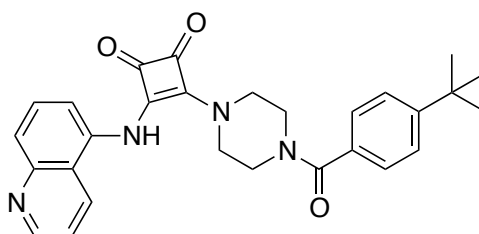
117
hP2X7R pIC₅₀ = 6.9
rP2X7R pIC₅₀ = 7.0



118
hP2X7R pIC₅₀ = 6.7

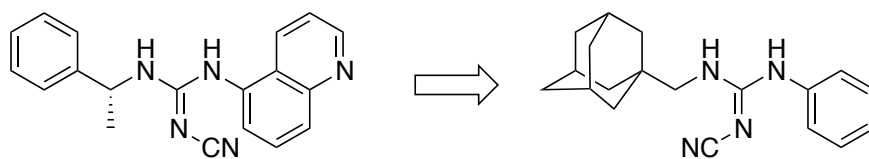


119
hP2X7R pIC₅₀ = 6.5



120
hP2X7R pIC₅₀ = 7.62

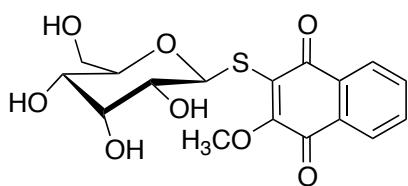
Fig. (25). P2X7R antagonists with cyanoguanidine structure



A-804598

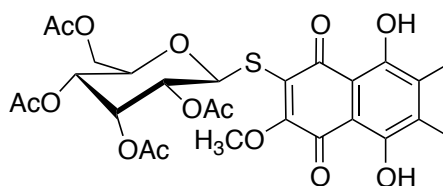
compound **121**

Fig. (26). 1,4-Naphthoquinones thioglycosides derivatives [138]



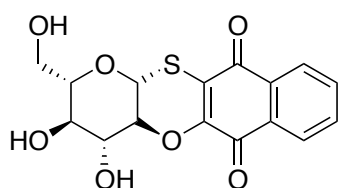
148

Ca²⁺ influx blockade 15%
YO-PRO-1 uptake blockade 35%



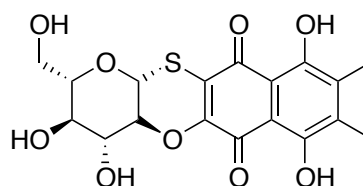
149

Ca²⁺ influx blockade 0%
YO-PRO-1 uptake blockade 25%



150

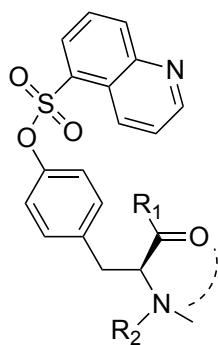
Ca²⁺ influx blockade 33%
YO-PRO-1 uptake blockade 43%



150

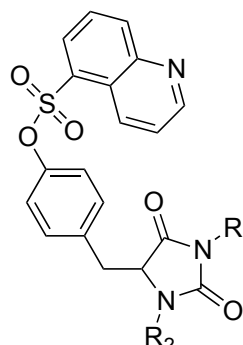
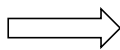
Ca²⁺ influx blockade 36%
YO-PRO-1 uptake blockade 18%

Fig. (27). Design of KN-62 analogs



KN-62

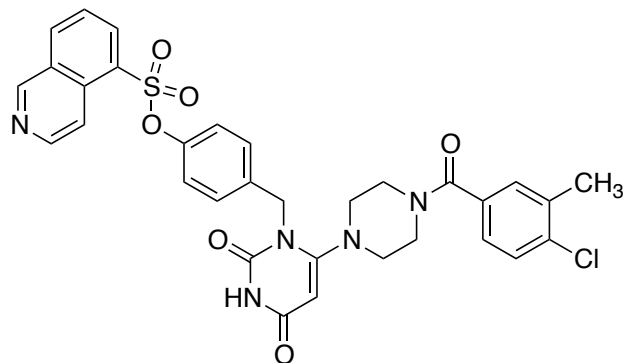
R₁= phenyl-4-piperazinyl
R₂= isoquinolin-5-sulfonyl



152

R₁= isoquinolin-5-ylmethyl
R₂= Boc-4-piperidinylmethyl

Fig. (28). Structure of compound **163**. The activity was assessed using the EtBr dye uptake inhibition assay [140]



163
hP2X7R IC₅₀ = 27 nM

Fig. (29). ^{11}C -labeled P2X7R PET radioligands

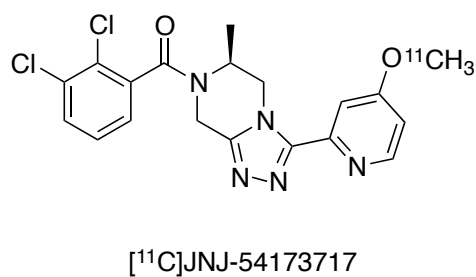
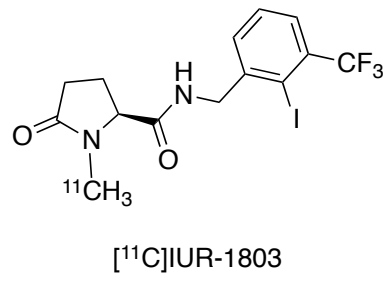
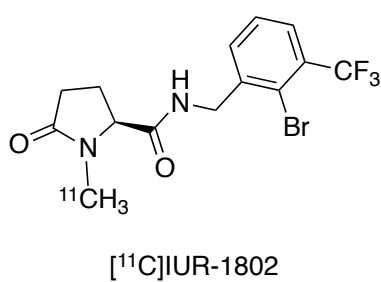
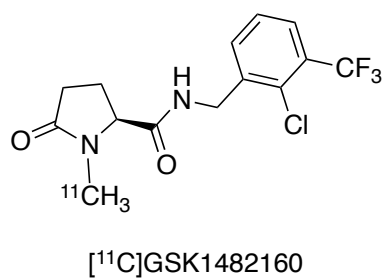
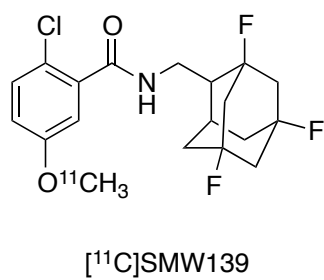
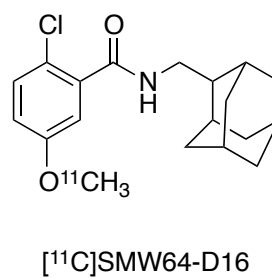
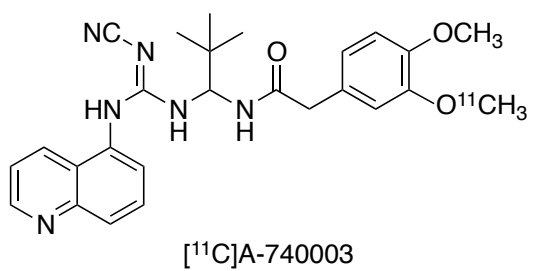
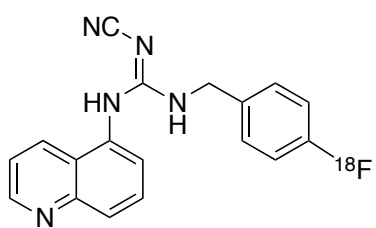
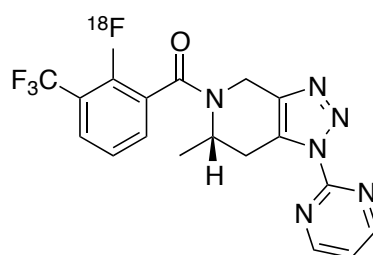


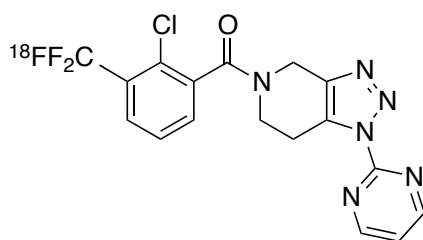
Fig. (30). ^{18}F -labeled P2X7R PET radioligands



$[^{18}\text{F}]\text{EFB}$

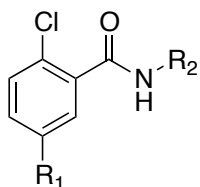


$[^{18}\text{F}]\text{JNJ64413739}$



$[^{18}\text{F}]\text{PTTP}$

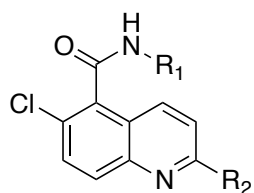
Table 1. Activity data of CNS-penetrant 2-Cl-benzamides **5-7** [97]



Compd	R ₁	R ₂	hP2X7R IC ₅₀ (nM) ^a
5	 <chem>Cc1ccncc1*</chem>	 <chem>CC1(CO)CCCCC1*</chem>	32
6	 <chem>Cc1cc(F)nc1*</chem>	 <chem>CC1(CO)CCCCC1*</chem>	16
7	 <chem>Cc1cc(F)nc1*</chem>	 <chem>CC1(CO)C(F)(F)CCCC1*</chem>	27

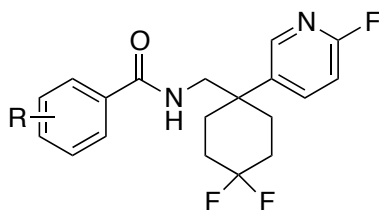
^aIC₅₀ values were determined from dye uptake inhibition assay in HEK-293 and THP-1 cells.

Table 2. Quinoline-based arylamides analogs **16-22** [103]



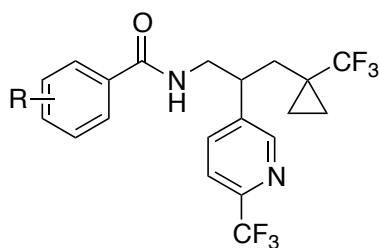
Compd	R ₁	R ₂	IC ₅₀ (nM) ^a			MDR-MDCK efflux ratio
			hP2X7R	rP2X7R	mP2X7R	
16		H	230	--	--	--
17			37	--	--	--
18			10	--	--	114
19			8.2	5100	2040	0.69
20			4.9	--	2000	1.8
21			19	4300	4830	8.7
22			4.5	640	1400	4.3

^aIC₅₀ values were determined using YO PRO dye uptake inhibition assay

Table 3. Benzamides derivatives **22-26** [105]

Compd	R	hP2X7R IC ₅₀ (nM) ^a
25	2,3-diCl	0.28
26	2-Cl-5-CH ₃	0.76
27	2,5-diCl	2.3
28	2,3-diF	290
29	2,3-diF	1500

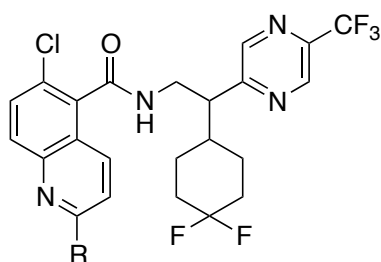
^aIC₅₀ values were determined from dye uptake inhibition assay in HEK-293 cells.

Table 4. Activity data of benzamide derivatives **30-32** [106]

Compd	R	hP2X7R IC ₅₀ (nM) ^a
30	2-Cl	0.09
31	2,3-diCl	10
32	2-F	430

^aIC₅₀ values were determined from dye uptake inhibition assay in HEK-293 cells.

Table 5. P2X7R activities of 6-chloro-quinoline-5-carboxamide derivatives **34-36** [110]



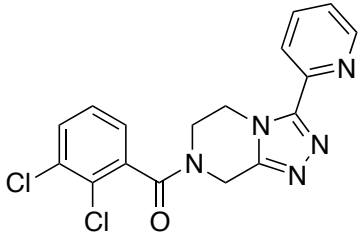
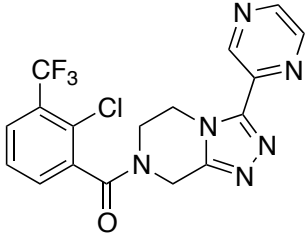
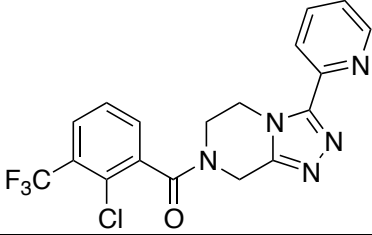
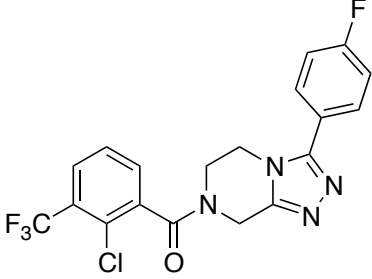
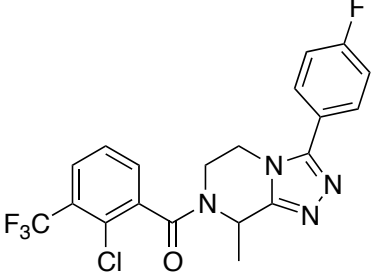
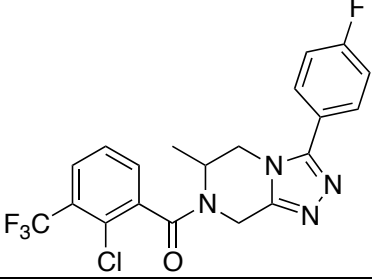
Compd	R	hP2X7R IC ₅₀ (nM) ^a	mP2X7R IC ₅₀ (nM) ^a
34		35	80
35		151	ND ^b
36		25	103

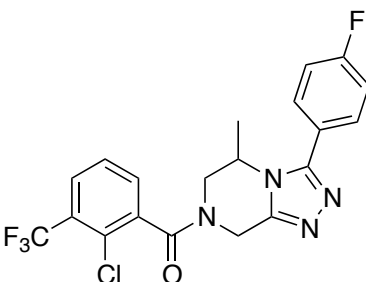
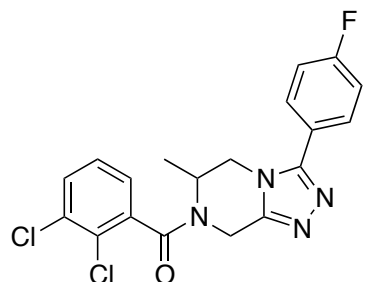
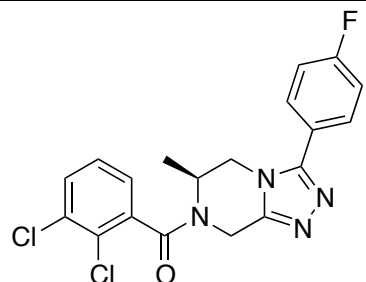
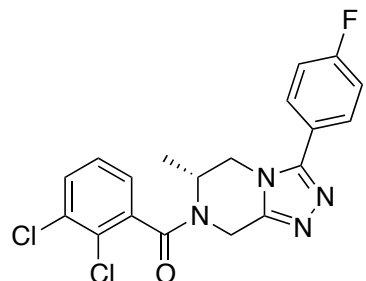
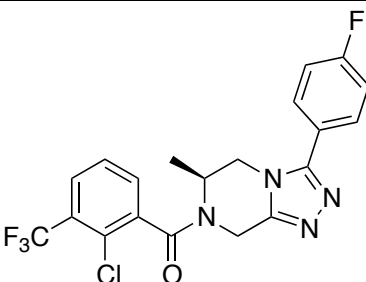
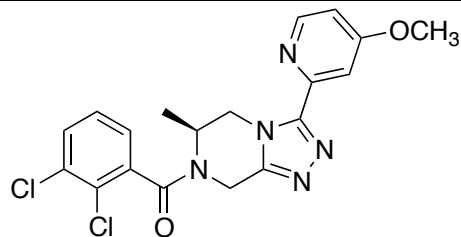
^aIC₅₀ values were determined using a FLIPR Ca²⁺ flux assay. ^bND = Not Determined.

Table 6. Activity at hP2X7R of rigidified arylbenzamides developed by GSK [111]

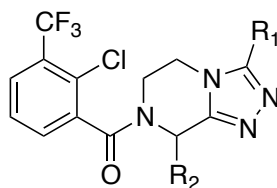
$6.5 < pIC_{50} < 7.0$		$pIC_{50} > 8.0$	
Compd	Structure	Compd	Structure
37		43	
38		44	
39		45	
40		46	
41		47	
42		48	

Table 7. 1,2,4 Triazole-5,6-dihydropyrazine benzamides **49-57** [112]

Compd	Structure	IC ₅₀ (nM) ^a	
		hP2X7R	rP2X7R
49		7.9	4430
50		2.1	92
51		9.7	1310
52		13.5	6390
53		10	7450
54		29	160

55		1370	1176
56		14	1230
S-56		7.7	8.8
R-56		1560	2240
S-54		8.7	14
57 JNJ-54173717		7.7	10

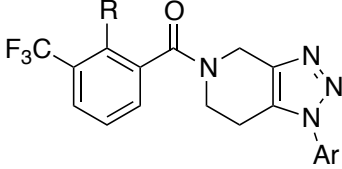
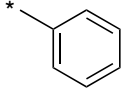
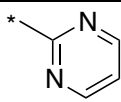
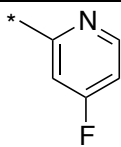
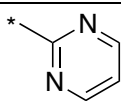
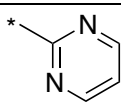
^aIC₅₀ values were measured in a FLIPR Ca²⁺ flux assay

Table 8. Activity data of 1,2,4 triazole-5,6-dihydropyrazine-based arylamides **58-62** [113]

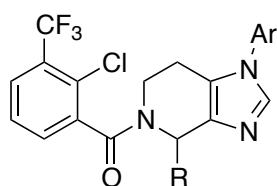
Compd	R ₁	R ₂	IC ₅₀ (nM) ^a		Efflux ratio
			hP2X7R	rP2X7R	
58	H		13	3065	--
59			12	43	--
60		CH ₃	>10000	>10000	--
61	CH ₃		2.7	27	5.10
62	CF ₃		8.8	82	0.75

^aIC₅₀ values determined in a FLIPR Ca²⁺ flux assay

Table 9. Activity data of 1,2,3-triazolopiperidine derivatives **63-67** [114]

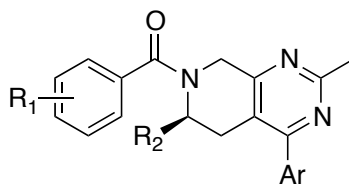
				
Compd	R	Ar	IC ₅₀ (nM) ^a	
			hP2X7R	rP2X7R
63	Cl		2.7	1900
64	Cl		4.2	6.8
65	Cl		2.1	30
66	F		22	258
67	CH ₃		2.2	349

^aIC₅₀ values were measured in a FLIPR Ca²⁺ flux assay

Table 10. Activity data of imidazopyridine derivatives **68-72** developed by Janssen [116]

Compd	R	Ar	IC ₅₀ (nM) ^a	
			hP2X7R	rP2X7R
68	H		4	609
69	H		9	1782
70	CH ₃		78	1182
71	CH ₃		14	592
<i>R-71</i>	CH ₃		4	115
<i>R-72</i>	CH ₃		15	116

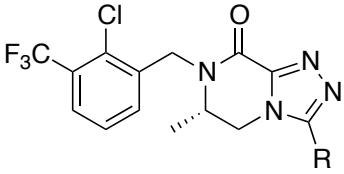
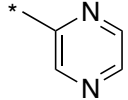
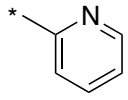
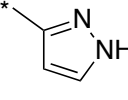
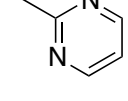
^aIC₅₀ values were measured in a FLIPR Ca²⁺ flux assay

Table 11. Activity data of pyrido-pyrimidines **75-78** [117]

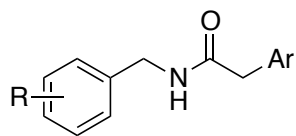
Compd	R ₁	R ₂	Ar	IC ₅₀ (nM) ^a	
				hP2X7R	rP2X7R
75	2-Cl-3CF ₃	H		8.5	1104
76	2-Cl-3CF ₃	H		110	21
77	2-Cl-3CF ₃	CH ₃		11	10
78	2-F-4Cl	CH ₃		19	17

^aIC₅₀ values were measured in a FLIPR Ca²⁺ flux assay

Table 12. Activity data for N-benzyl lactam derivatives *S-80-S-83* [118]

			
		IC₅₀ (nM)^a	
Compd	R	hP2X7R	rP2X7R
<i>S-80</i>		0.7	79
<i>S-81</i>		0.5	350
<i>S-82</i>		0.6	7.1
<i>S-83</i>		0.5	32

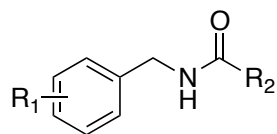
^aIC₅₀ values were measured in a FLIPR Ca²⁺ flux assay

Table 13. Activity data of compounds **94-98** [125]

Compd	R	Ar	hP2X7R IC ₅₀ (nM) ^a
94	2,4-diCl		8.1
95	2-Cl,3-CF ₃		8.6
96	2-Cl,4-F		8.0
97	2-Cl,4-F		7.9
98	2-Cl,4-F		6.8

^aIC₅₀ values were determined by using an ethidium bromide release assay.

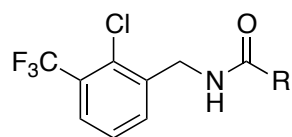
Table 14. P2X7R activity data for aliphatic amide derivatives **101-108** [128]



Compd	R ₁	R ₂	hP2X7R pIC ₅₀ ^a	Compd	R ₁	R ₂	hP2X7R pIC ₅₀ ^a
101	2-Cl,4-F		7.0	105	2-Cl,4-F		7.5
102	2-Cl,4-F		7.5	106	2-Cl,4-F		8.2
103	2-Cl,4-F		7.0	107	2-Cl,3-CF ₃		8.6
104	2-Cl,4-F		<6	108 GSK- 1482160	2-Cl,3-CF ₃		8.5

^apIC₅₀ values were determined by using ethidium bromide uptake assay.

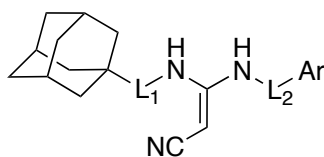
Table 15. SAR data for 2-oxoimidazolidine-4-carboxamide derivatives **109-114** [129]



Compd	R	hP2X7R pIC ₅₀ ^a	Rat CL _{int} (mL/min/g)	Compd	R	hP2X7R pIC ₅₀ ^a	Rat CL _{int} (mL/min/g)
109		9.2	<0.5	112		8.4	0.6
110		8.4	0.7	113		7.6	4.4
111		7.8	--	114		8.4	0.9

^apIC₅₀ values were determined by using ethidium bromide uptake assay.

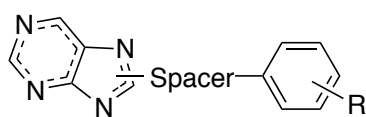
Table 16. Activity data for cyanoguanidines **121-132** [134]



Compd	L ₁	L ₂	Ar	hP2X7R IC ₅₀ (nM) ^a	Compd	L ₁	L ₂	Ar	hP2X7R IC ₅₀ (nM) ^a
121	CH ₂	--		100	127	CH ₂	--		174
122	--	--		2455	128	CH ₂	--		562
123	(CH ₂) ₂	--		>10000	129	CH ₂	CH ₂		501
124	CH ₂	CH ₂		407	130	CH ₂	--		>10000
125	CH ₂	--		51	131	CH ₂	CH ₂		69
126	CH ₂	--		58	132	CH ₂	--		18

^aIC₅₀ values were determined by using YO-PRO-1 dye uptake assay

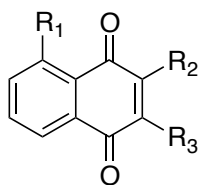
Table 17. Activity data of compounds **133-139** [135]

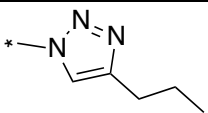
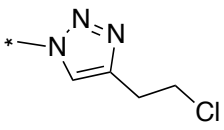


Compound		Spacer		hP2X7R (%) ^a
133				7
134				63
135				25
136				2
137				4
138				17
139				52

^a % inhibition at 10 μ M of YO-PRO-1 dye uptake in hP2X7-HEK293 cells stimulated with BzATP (30 μ M)

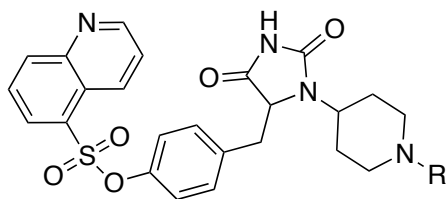
Table 18. Activity data of 1,4-naphthoquinone derivatives **140-147** [136,137]



Compd	R ₁	R ₂	R ₃	hP2X7R IC ₅₀ (nM) ^a	mP2X7R IC ₅₀ (nM) ^a
140	H	OH	H	--	>10000
141	H	OH	Br	412	712
142	H	OH	I	71	48.4
143	H	OH	Ph	22	23.1
144	H	OH	4-CH ₃ -Ph	--	>10000
145	H	OH	3-F-Ph	--	>10000
146	OH		H	230	--
147	OH		H	103	--

^aIC₅₀ values were determined by using dye uptake assay

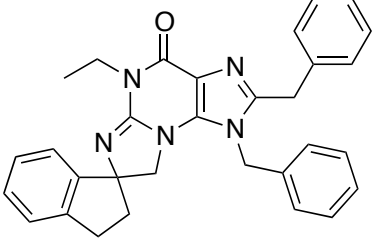
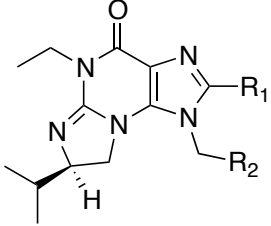
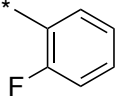
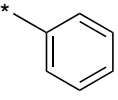
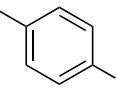
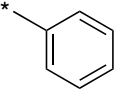
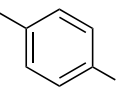
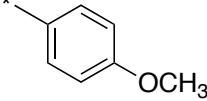
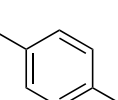
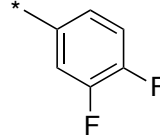
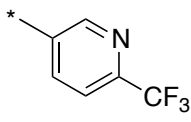
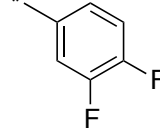
Table 19. Activity data of KN-62-inspired rigid analogs **153-162** [139]



Compd	R	hP2X7R IC ₅₀ (μM) ^a	Compd	R	hP2X7R IC ₅₀ (μM) ^a
153	H	NA ^b	158		0.574
154		11.7	159		0.7
155		4.9	160		0.07
156		2.3	161		0.07
157		0.02	162		0.217

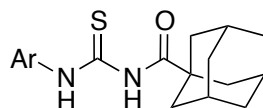
^aIC₅₀ values were determined using EtBr dye uptake inhibition assay. ^bNA= Not Active

Table 20. Structural modifications of the N-1 and C-2 position of arylamide guanine-based compounds [141]

 164				
Compd	R ₁	R ₂	hP2X7R IC ₅₀ (nM) ^a	IL-1β IC ₅₀ (nM) ^b
165			439	NA ^c
166			141	2752
167			NA	NA
168			29	295
169			50	82

^aIC₅₀ determined using FLIPR Ca²⁺ flux assay. ^bIC₅₀ determined using human whole blood assay.

^cNA= Not Active.

Table 21. Activity data and selectivity for adamantane-1-carbonyl thiourea derivatives [142]

Compd	Ar	hP2X7R IC ₅₀ (μM) ^a (% inhibition)
170		1.474
171		(19%)
172		1.395
173		0.699
174		0.099
175		0.073

^aIC₅₀ determined using a FLIPR Ca²⁺ flux assay.